Science of the Total Environment 787 (2021) 147858

Contents lists available at ScienceDirect

Science of the Total Environment

journal homepage: www.elsevier.com/locate/scitotenv

Aragonite saturation state in a continental shelf (Gulf of Cádiz, SW Iberian Peninsula): Evidences of acidification in the coastal area

Dolores Jiménez-López *, Teodora Ortega, Ana Sierra, Rocío Ponce, Abelardo Gómez-Parra, Jesús Forja

Dpto. Química-Física, INMAR, Facultad de Ciencias del Mar y Ambientales, Universidad de Cádiz, Campus Universitario Río San Pedro, 11510 Puerto Real, Cádiz, Spain

HIGHLIGHTS

- Hydrodinamical conditions determine the spatial variability of ΩAr in surface waters.
- Biological processes control ΩAr changes in SML.
- In deep waters, the lowest ΩAr values are related to $NACW_P$.
- ΩAr and pH have decreased in the coastal areas between 2006 and 2016.

GRAPHICAL ABSTRACT

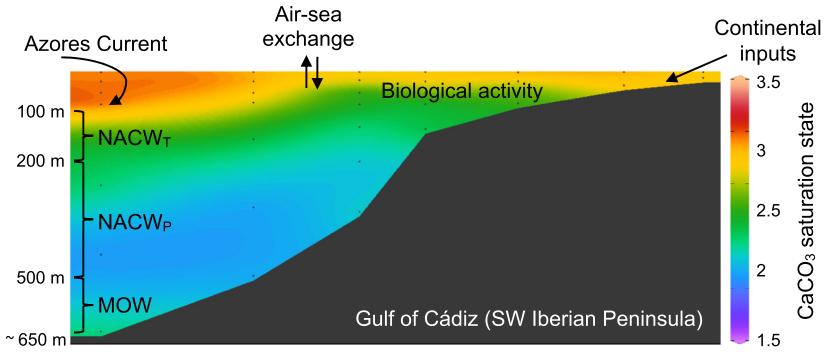

ARTICLE INFO

Article history:
Received 30 November 2020
Received in revised form 1 May 2021
Accepted 14 May 2021
Available online 20 May 2021

Guest Editor: Víctor M. León

Keywords:
Calcium
Total alkalinity
Aragonite saturation state
Ocean acidification
Gulf of Cádiz

ABSTRACT

The spatiotemporal variability of aragonite saturation state (ΩAr) has been studied in the eastern shelf of the Gulf of Cádiz (GoC) (SW Iberian Peninsula). The study was carried out during the years 2014 and 2016 aboard twelve oceanographic cruises, along three or five transects, located between Cape Trafalgar and the Guadiana River. The GoC exhibited oversaturated of calcium carbonate with ΩAr mean values of 2.68 ± 0.30 in surface and 2.05 ± 0.15 in deep waters. pH, total alkalinity (TA), calcium concentration (Ca^{2+}) and ΩAr showed a high variability within the surface mixed layer (SML, z < 100 m). Biological activity seemed to be the main process to determine the ΩAr variability in the SML, revealing a greater importance than temperature, mixing or air-sea processes. The buffer factors of the CO_2 system in the GoC have been estimated in the SML waters, and they are related with the biological activity and the temperature changes. A decrease of pH and ΩAr in this SML with depth was observed, due to the increase of the respiratory processes. In deep waters (z > 100 m), TA and Ca^{2+} concentration presented a conservative behaviour related to the distribution of the different water masses located in the GoC. The vertical variation of ΩAr also depends on the degree of mineralization of these water masses, obtaining the maximum values in the Subtropical North Atlantic Central Water (100–200 m), minimum values in the Subpolar North Atlantic Central Water (about 400 m), and intermediate values associated to the presence of the Mediterranean Water (>500 m). Results showed a significative acidification of the coastal areas, for those depths lower than 100 m from 2006 to 2016, with a mean decrease of pH and ΩAr of −0.0089 and −0.0552 yr^{-1}, respectively.

1. Introduction

The concentration of carbon dioxide (CO_2) in Earth's atmosphere has been in continuous increase since the beginning of the industrial era, when the concentration was of 278 ppm in 1750 (Joos and Spahni,

* Corresponding author.
E-mail address: dolores.jimenez@uca.es (D. Jiménez-López).

https://doi.org/10.1016/j.scitotenv.2021.147858

2008), to approximately 411 ppm in October 2020 (Earth System Research Laboratories, https://www.esrl.noaa.gov/gmd/ccgg/trends/mlo.html). This CO_2 increase is mainly due to the rise of anthropogenic activities, such as, fossil fuel combustions and land use changes. In consequence, this will lead to pronounced variations in our climate by the end of this century (Siegenthaler et al., 2005). The oceans act as the major sinks for this increasing atmospheric CO_2. It has been estimated, based on the 2019 assessment of the Global Ocean Project, that over the decade 2009–2018 oceans have absorbed about 23 ± 5% (2.6 ± 0.5 PgC yr^{-1}) of the total CO_2 emissions (Hauck et al., 2020). This has significantly benefitted humankind by reducing the greenhouse gas levels in the atmosphere (Sabine and Feely, 2007). Hence, the fundamental role of the oceans as buffers of natural and anthropogenic CO_2 emissions, as well as, in mitigating climate change (Landschützer et al., 2019).

The changes caused in the seawater carbonate chemistry with impacts on its chemical speciation and biogeochemical cycles by the CO_2 uptake from the atmosphere, is referred to a phenomenon known as: ocean acidification (OA) (e.g. Doney et al., 2009; Ríos et al., 2015; Wanninkhof et al., 2015). An increase of CO_2 in surface waters leads to a decrease of the ocean's buffering capacity, due to a decrease in pH, carbonate ions (CO_3^{2-}) concentrations and the calcium carbonate ($CaCO_3$) saturation state. Global surface ocean pH is projected to decrease by ~0.33 ± 0.04 units within this century (Jiang et al., 2019) and 0.7 units in the next 300 years (Caldeira and Wickett, 2005). This pH drop-off can inhibit the capacity of many marine organisms to form $CaCO_3$ skeletons and shells (Orr et al., 2005; Gattuso et al., 2015). Marine organisms affected by this OA include open-ocean species, such as foraminifera, coccolithophores and pelagic mollusks, among others. Nevertheless, the greatest concern is with the coastal calcifying organisms, including bivalves, shallow-water calcareous algae and especially corals (Doney, 2006; Doney et al., 2009). However, some organisms could present certain resistance to OA effects (Ries et al., 2009; Dupont et al., 2010; Aberle et al., 2013), which in turn depends on other factors, such as, temporal dynamics, species-specific thermal tolerances and food availability (Ramajo et al., 2016; Leung et al., 2019), that are not incorporated into the models and can add uncertainty to these estimates (Bindoff et al., 2019).

In continental shelves and coastal systems, the decrease of pH over time is much more pronounced than in open oceans. This is due to the fact that these areas are not only affected by global OA caused by increasing atmospheric CO_2 levels. These systems are also influenced by the coupled effects of various processes, such as, the mixing between freshwater and seawater, the eutrophication, the upwelling, the organic matter degradation and the biological activity, being the pH controlling mechanisms more complex than in the open ocean (Feely et al., 2010; Cai et al., 2011; Duarte et al., 2013; Zhai et al., 2014; Xue et al., 2016; Hu et al., 2017). In this sense, Carstensen and Duarte (2019) found a much broader range of trends in 83 coastal systems across the world (−0.023 to 0.023 pH units yr^{-1}), resulting larger than the one estimated for oceanic times series (−0.0004 to −0.0026 pH units yr^{-1}). In addition, the coastal contributions of nutrients and carbon, the intense biological activity (photosynthesis/respiration) and the greater influence of benthic fluxes in the water column cause a greater spatial and seasonal variability of pH, different carbonic species concentrations and degree of $CaCO_3$ saturation (e.g. Wootton et al., 2008; Carstensen and Duarte, 2019).

Aragonite is usually the most abundant form of biogenic $CaCO_3$ in seawater. It is approximately 1.5 times more soluble than calcite (Millero, 2007; Wanninkhof et al., 2015). Therefore, the saturation state of aragonite (ΩAr) can be considered as a good indicator to study the marine carbonate system, regarding that if $\Omega Ar < 1$ the dissolution of aragonite shells and skeletons is favoured (Feely et al., 2009). Moreover, the aragonite is essential for many phytoplanktonic and benthonic species (Gattuso et al., 2015; Waldbusser et al., 2015), and it is also the main $CaCO_3$ form in shallow waters (Mucci, 1983; Morse et al., 2006, 2007). Taking this into account, the studies of ΩAr have received special interest in the last few years (Feely et al., 2010; Hu et al., 2017; de Carvalho-Borges et al., 2018; Cotovicz et al., 2018). For this reason, ΩAr has also been used to assess the effects of natural processes and human activities on marine calcareous organisms in coastal waters (Zhai et al., 2014; Xue et al., 2017; Eyre et al., 2018: Li and Zhai, 2019; Zhai et al., 2020).

The Gulf of Cádiz (GoC) is strategically located by its proximity to the Strait of Gibraltar. It plays a key role in the carbon cycle of the eastern part of the North Atlantic (Parrilla, 1998) and Mediterranean Sea (Dafner et al., 2001), and receives several continental inputs from different rivers. Still, there are very few studies focussed on the spatiotemporal variability of the carbonate system and $CaCO_3$ saturation state in this area. They are generally designed to know if the GoC acts as source or sink of CO_2 or to estimate the amount of anthropogenic carbon that is exchanged between the Mediterranean Sea and the Atlantic Ocean (Aït-Ameur and Goyet, 2006; Huertas et al., 2006, 2009; de la Paz et al., 2008, 2011; Ribas-Ribas et al., 2011; Flecha et al., 2012; Jiménez-López et al., 2019). Ribas-Ribas et al. (2011) showed that the temporal and spatial variability in the distribution of inorganic carbonate system parameters in the northeastern shelf of the GoC was controlled by river inputs, primary production, respiration, CO_2 air-sea exchange and remineralization. Also, Flecha et al. (2019) completed a study of a decadal trend (from 2005 to 2015) of the carbonate system parameters in the different exchanging water masses in the Strait of Gibraltar, concluding that the contribution of the anthropogenic driver was responsible for about 40% of the pH changes.

The OA in oceanic waters has been focus of many studies, but little is known regarding to its status in coastal waters (coastal and continental shelf systems). So, the main aim of this paper is to evaluate the spatiotemporal variability of $CaCO_3$ saturation state between the years 2014 and 2016. In addition, this study will also estimate the decadal evolution (2006–2016) of the carbonate system parameters in the shallowest waters of the GoC, as well as the influence of OA in the pH and ΩAr changes, using the dataset obtained by Ribas-Ribas et al. (2011) in the northeastern shelf of this area between 2006 and 2007.

2. Material and methods

2.1. Study area

The study was carried out in the GoC, located in the southwestern Iberian Peninsula (Fig. 1). Water circulation in this area is characterized by the bilayer exchange that takes place in the Strait of Gibraltar due to the density differences between two water masses: an inflow of Atlantic water on the surface towards the Mediterranean basin, and a deeper outflow of Mediterranean water that courses into the Atlantic Ocean (e.g. Baringer and Price, 1999; Sánchez-Leal et al., 2017). This same circulation pattern is found in the GoC with the distribution of three main water masses at different depth intervals (Criado-Aldeanueva et al., 2006; Bellanco and Sánchez-Leal, 2016). The Surface Atlantic Water (SAW) that extends at the shallowest depths up to the seasonal thermocline, with coastal and atmospheric interaction. The North Atlantic Central Water (NACW), at an intermediate depth below 100 m in two different varieties, $NACW_T$, a warmer water mass of subtropical origin, and $NACW_P$, a colder one of subpolar origin (Pérez et al., 2001). The Mediterranean Outflow Water (MOW) that flows between 300 and 400 m deep from the seafloor within the Strait of Gibraltar and spills over the slope of the GoC (Carracedo et al., 2016).

Furthermore, due to its importance, this work also focused on the Guadalquivir system (Fig. 1). The Guadalquivir River has a length of 680 km and a drainage basin of 63,822 km^2 (Granado-Lorencio, 1991). This estuary extends up to 110 km from its mouth to the Alcalá del Río dam with a semidiurnal tidal period (Díez-Minguito et al., 2013), and it is clearly affected by anthropogenic activity (Huertas et al., 2005; de la Paz et al., 2007; Ruiz et al., 2015). The Guadalquivir

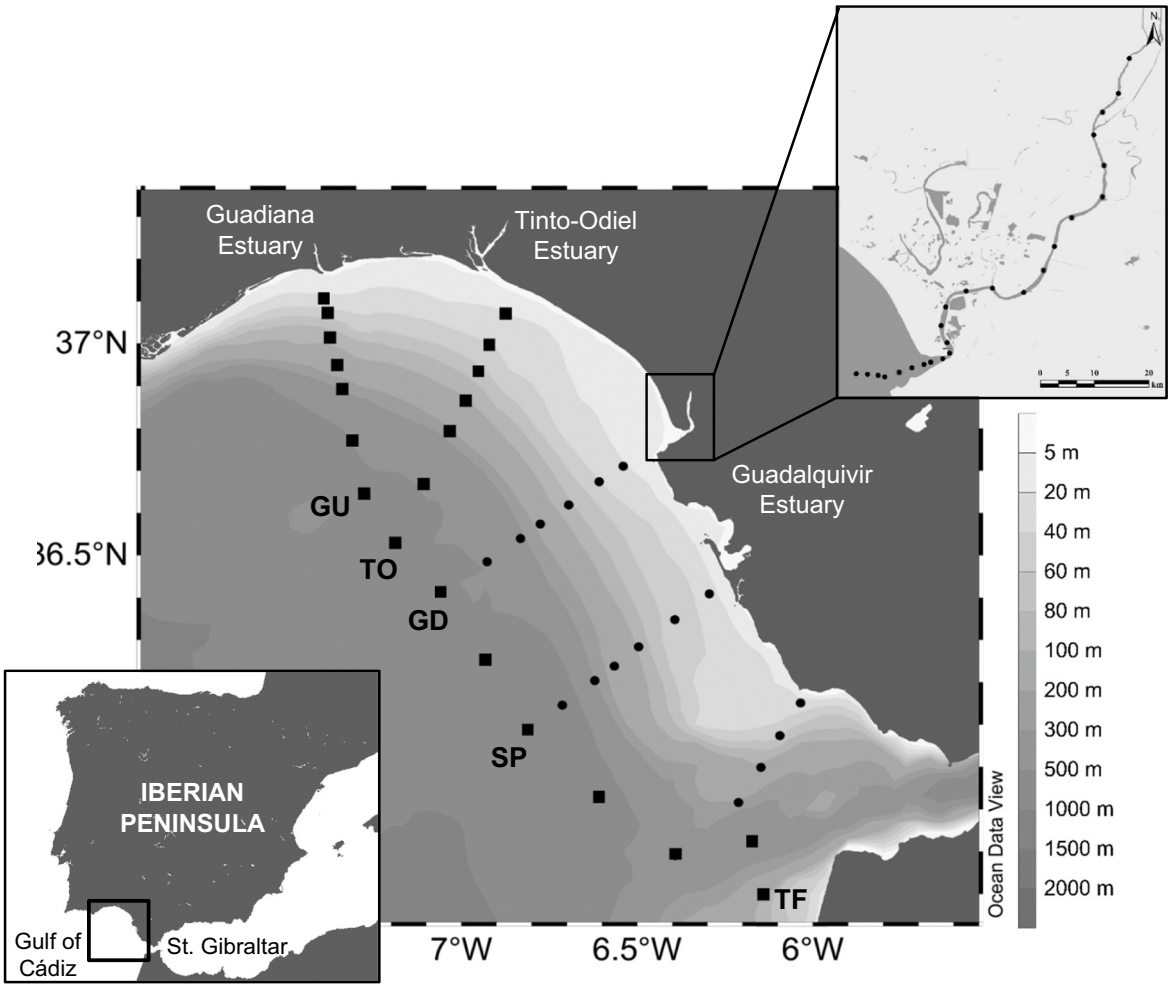

Fig. 1. Map of the Gulf of Cádiz showing the location of sampling stations during the cruises followed in STOCA (dots) and OCAL (squares) projects, along five transects: Trafalgar (TF), Sancti Petri (SP), Guadalquivir (GD), Tinto-Odiel (TO) and Guadiana (GU), in addition to three offshore stations. The sampling stations in the Guadalquivir estuary are also displayed.

River is the responsible of the main freshwaters discharges to the GoC with an annual input of 1.5×10^9 m^3 approximately (Confederación Hidrográfica del Guadalquivir, España, n.d.; http://www.chguadalquivir.es/saih/DatosHistoricos.aspx).

2.2. Field sampling and analytical methods

The sampling was conducted through two projects (STOCA and OCAL) and twelve cruises were carried out on board the R/V's Ángeles Alvariño and Ramón Margalef between 2014 and 2016, at the beginning of each season (March, June, October and December). Samples were taken at different depths in fixed stations, which were distributed along transects perpendicular to the coastline. On the one hand, the STOCA project was developed over 34.1×10^2 km^2, with a total number of sixteen stations distributed in three transects, Trafalgar transect (TF), Sancti Petri transect (SP) and Guadalquivir transect (GD) (Fig. 1), with a total number of 578 samples. On the other hand, the OCAL project covered a more extensive area of the GoC, 69.1×10^2 km^2, including thirty-seven sampling stations along two additional transects, Tinto-Odiel transect (TO) and Guadiana transect (GU) (Fig. 1), with a total of 766 samples.

In addition, five other cruises were carried out in the Guadalquivir estuary on board of the R/V UCadiz during July 2017, March and April 2018, as well as March and April 2019. The sampling strategy covered a longitudinal transect across the river with a total of twenty five stations for each cruise (Fig. 1).

Seawater samples to analyse pH, total alkalinity (TA) and calcium concentrations ($[Ca^{2+}]$) were collected using Niskin bottles (10 L). These were mounted on a rosette-sampler coupled to a Seabird CTD 911+, which measured temperature (T), practical salinity (S_P) and dissolved oxygen (DO). T and S_P measurements resulted with an accuracy better than ±0.005 °C and ±0.02 units, respectively. DO values were obtained from the sensor included in the rosette (SBE 63), which was pre-calibrated with several water depths samples at selected stations using Winkler titration (±0.1 μmol kg^{-1}) (Parsons et al., 1984). Apparent oxygen utilization (AOU) was defined as the difference between the calculated solubility applying the Benson and Krause Jr. (1984) expression and the measured DO values.

Water samples for pH and TA measurements were obtained from Niskin bottles following the protocol described in SOP1 (Dickson et al., 2007) and they were preserved in 500 mL borosilicate glass bottles ensuring no headspace, and stored in darkness at constant temperature until its analysis on board. The total suspended matter in the GoC is lower than 0.5 mg L^{-1} (Freitas and Abrantes, 2002), and the possible interference on TA analysis could be relatively unappreciable. Nevertheless, the corresponding samples to the Guadalquivir estuary were filtered through pre-combusted glass-fibre filters (Whatman, GF/F 0.7 μm) immediately after sampling due to the high turbidity. Both measurements were performed in duplicate within a period of less than 4 h from the sampling.

pH was measured with a potentiometer, using a glass-combined electrode (Metrohm, 6.0253.100) calibrated on the total pH scale with a TRIS buffer solution (Zeebe and Wolf-Gladrow, 2001). This electrode

was calibrated, approximately, every fifteen samples in order to obtain a right accuracy of pH measurement. The precision for these pH measurements was determined from regular measurements by means of two batches (Batch # 128 and 153) of Certified Reference Material (CRM supplied by Prof. Andrew G. Dickson, Scripps Institute of Oceanography, San Diego, USA). Results showed a precision of ±0.003 ($n = 15$) for measurements obtained in the laboratory under controlled temperature conditions, and ±0.005 ($n = 65$) for those carried out on board. Prior to this, pH was normalized to 25 °C using the CO2SYS program (Pierrot et al., 2006) including the K1 and K2 acidity constants proposed by Millero (2010) in the pH total scale, the HSO_4^- constant of Dickson (1990) and the total boron constant of Lee et al. (2010). TA measurements were obtained by potentiometric titration (Metrohm, 905) with standardized 0.1 M HCl (0.7 mol kg^{-1} in NaCl), using a fixed sample volume of 96.570 ± 0.008 mL. TA values were converted to μmol kg^{-1} through the seawater density (Millero and Poisson, 1981) to the in situ T and S_P. The titration of CRMs (Batch # 128 and 153) was used to test the titration system. Thus, an accuracy of ±3 μmol kg^{-1} and a precision of ±3 μmol kg^{-1} was obtained in the TA measurements (n = 65). The analytical performance of pH and TA resulted in agreement with the oceanographic data described by Olsen et al. (2019). Moreover, pH and TA were used in the CO2SYS program (Pierrot et al., 2006) to calculate pH at in situ T (pH_T), dissolved inorganic carbon (DIC) and CO_3^{2-} concentrations in the same conditions described for the pH normalization. Phosphate (PO_4^{3-}) and silicate (SiO_2) concentrations were also included in the CO2SYS calculations.

Ca^{2+} samples were stored and refrigerated at a constant temperature until their later analysis in the laboratory. [Ca^{2+}] were measured in duplicate after weighing the water sample (~5 g, ±0.0001 g), by classic volumetric titration with ethylene glycol tetraacetic acid (EGTA, 0.01 M) as titrant and borax (0.1 M) as a buffer (~10 mL), and using a calcium selective electrode (Metrohm, 6.0510.100). This method is described by Rosón et al. (2016) and the references are included therein. A [Ca^{2+}] standard (~10 mmol kg^{-1}) was prepared dissolving 1.00664 ± 0.00001 g of pure $CaCO_3$ in a 1000.0 ± 0.5 mL analytical flask. In order to reach the seawater ionic strength, 29.131 ± 0.001 g of NaCl and 5.349 ± 0.001 g of $MgCl_2$ were added (both free of calcium impurities), as well as several additions of 0.5 mL of HCl 12 N up to 6.5 mL to ensure the complete $CaCO_3$ dissolution. A reproducibility of ±3 μmol kg^{-1} was obtained with this method, obtained from the average of the standard deviations of the duplicated measurements. Additionally, before analysing the Ca^{2+} in samples, in order to check the precision of this method, some regular measurements (n ≈ 5) were carried out from two standard samples daily (Batch # 128 and 153), giving a global value of ±5 μmol kg^{-1} ($n = 120$). During the STOCA cruises, [Ca^{2+}] was not measured, instead it was determined by means of the experimental relationship between [Ca^{2+}] and S_P obtained from the OCAL cruises measurements, which were below the thermocline depth ([Ca^{2+}]/S_P = 293.3 (±0.4) μmol kg^{-1}, $r^2 = 0.93$, $n = 256$). ΩAr was determined through [CO_3^{2-}] and [Ca^{2+}], and the apparent solubility product for aragonite (Mucci, 1983), but taking into account the pressure correction proposed by Millero (1979).

Finally, nutrient samples for analysis of nitrate (NO_3^-), PO_4^{3-} and SiO_2 contents were filtered through pre-combusted glass-fibre filters (Whatman, GF/F 0.7 μm) and stored at −20 °C until their later analysis in the laboratory. Analyses were performed in a segmented flow autoanalyser (Skalar, San Plus) based on classic spectrophotometric methods (Grasshoff et al., 1983). The accuracies were of ±0.10 μmol L^{-1} for NO_3^-, ±0.02 μmol L^{-1} for PO_4^{3-} and ±0.05 μmol L^{-1} for SiO_2. Chlorophyll-a (Chl) values for the different cruises were obtained from González-García et al. (2018) and González-García et al., submitted.

2.3. Calculations

The contributions of temperature, air-sea exchange, mixing and in situ biological activity processes to seasonal ΩAr net changes have been calculated in the surface mixed layer (SML, z < 100 m) using a mass budget model proposed by Xue et al. (2017). This method has been applied independently using the mean values in coastal (bottom depth < 100 m) and distal (bottom depth > 100 m) areas (n = 12, see Figs. S1 and S2 in Supplementary material).

In addition, in order to quantify the ability of the GoC waters to resist changes in the CO_2 system, we have estimated the buffer factor changes in the CO_2 system using the formulation presented by Álvarez et al. (2014) based on Egleston et al. (2010), also differing between coastal and distal areas in the SML. The three factors studied quantify the sensitivity of aqueous CO_2 (γ_{DIC}), hydrogen ion concentration or activity (β_{DIC}) and the carbonate saturation state Ω (ω_{DIC}) of changes in DIC when the TA parameter is kept constant. The Revelle factor (R), has also been directly calculated as DIC/γ_{DIC} (Egleston et al., 2010) (Table S1 and Fig. S3, see in Supplementary material). Note that higher absolute values of buffer factors indicate a greater buffer capacity, whereas higher R values indicate decrease in the seawater buffering capacity.

An Optimum Multiparameter Analysis (OMP) has been applied in our study area to identify the spatial distribution and mixing proportions of water masses. This method is an extension of the classical analysis based on T and S_P variables, including biogeochemical variables, such as oxygen or nutrients as a new feature (Tomczak Jr., 1981; Tomczak and Large, 1989; Karstensen and Tomczak, 1998; Poole and Tomczak, 1999). The OMP analysis was used to determinate the contribution of the different water masses to each sample, represented as a percentage. This analysis was performed during the OCAL cruises, and in order to avoid the mixing layer effect in our study area only samples below a depth of 100 m were used ($n = 256$). Three water masses were included, $ENACW_P$, $ENACW_T$ and MOW and the analysis was applied taking into account the conservative (T, S and SiO_2) and non-conservative variables (DO, NO_3^-, PO_4^{3-}). Moreover, the values described by Flecha et al. (2012) were used to define the source water types of our study area. This included performed TA calculated for NACW according to Pérez et al. (2002) and in the case of MOW, those established by Rhein and Hinrichsen (1993), as well as Santana-Casiano et al. (2002). Moreover, from the results of the water masses distribution obtained with this OMP approach, the values of a particular variable can be estimated by iterative solving the set of equations involved (256 linear equations). Therefore, the values of Ca^{2+}, TA and DO were estimated, and the derived variables of pH_T and ΩAr were computed using CO2SYS program, and AOU values were calculated with the solubility expression from Benson and Krause Jr. (1984).

2.4. pH and ΩAr variation in the GoC

Our data were compared to the database performed by Ribas-Ribas et al. (2011) followed in the coastal waters of the northeastern shelf of the GoC during four cruises that took place in June 2006, November 2006, February 2007 and May 2007. The study area was located 36.39–36.93°N and 6.83–6.25°W, with sixty-three sampling stations in each cruise and 989 samples in total at a maximum depth of 95 m. The main aim of this comparison was to study the variation of pH and ΩAr throughout eleven years in the coastal area of the GoC. To do this, we took into account the mean values of T, S_P, pH_T, TA and DIC for surface (z < 20 m) and subsurface waters (z > 20 m) measured by Ribas-Ribas et al. (2011) (Table 1 therein, distal waters). They were compared with the mean values of our work, at the stations with bottom depths lower than 100 m, and using the same approach of division between surface and subsurface waters. In addition, this variation study was carried out about pH_T and ΩAr values to the mean T registered among both works (17.1 °C) in order to avoid the possible effect caused by T changes (pH_T@Tmean and ΩAr@Tmean, respectively). This normalization was also followed by CO2SYS program in the same conditions described previously.

Table 1
Number of samples (n), mean values and standard deviations of practical salinity (S_P), temperature (T), apparent oxygen utilization (AOU), pH_T (pH at in situ temperature), total alkalinity (TA), dissolved inorganic carbon (DIC), calcium concentration (Ca^{2+}), and aragonite saturation state (ΩAr) measured at fixed stations for the different cruises undertaken between 2014 and 2016. Three vertical intervals are considered: surface (0–100 m), intermediate (100–500 m) and deep (>500 m). The depth range of the surface mixed layer (SML) is included in the first vertical interval.

Depth	Cruise	n	SML (m)	S_P	T (°C)	AOU (μmol kg^{-1})	pH_T	TA (μmol kg^{-1})	DIC (μmol kg^{-1})	Ca^{2+} (mmol kg^{-1})	ΩAr
Surface (0–100 m)	Spring 2014	58	5–100	36.1 ± 0.2	14.9 ± 0.6	7.2 ± 18.6	8.07 ± 0.03	2288 ± 15	2050 ± 28	10.60 ± 0.06	2.54 ± 0.19
	Summer 2014	65	15–75	36.2 ± 0.1	17.3 ± 2.5	7.5 ± 25.7	7.98 ± 0.04	2293 ± 24	2081 ± 29	10.61 ± 0.04	2.35 ± 0.34
	Autumn 2014	55	20–70	36.1 ± 0.1	18.7 ± 2.6	6.8 ± 23.1	8.00 ± 0.05	2290 ± 32	2060 ± 34	10.59 ± 0.03	2.51 ± 0.36
	Winter 2014	53	60–120	36.3 ± 0.2	17.6 ± 0.7	12.0 ± 8.8	8.04 ± 0.05	2319 ± 32	2068 ± 35	10.65 ± 0.04	2.69 ± 0.27
	Spring 2015	54	5–90	36.1 ± 0.1	14.8 ± 0.6	2.4 ± 20.4	8.08 ± 0.09	2332 ± 28	2084 ± 50	10.58 ± 0.03	2.63 ± 0.47
	Summer 2015	56	20–60	36.3 ± 0.1	18.6 ± 2.5	6.8 ± 20.6	8.02 ± 0.04	2339 ± 32	2091 ± 36	10.66 ± 0.04	2.68 ± 0.31
	Autumn 2015	56	20–40	36.1 ± 0.1	17.1 ± 2.5	18.6 ± 25.7	7.93 ± 0.05	2326 ± 30	2135 ± 33	10.60 ± 0.03	2.14 ± 0.34
	Winter 2015	54	20–75	36.4 ± 0.1	19.0 ± 1.8	5.6 ± 10.3	8.03 ± 0.01	2313 ± 13	2058 ± 16	10.68 ± 0.03	2.74 ± 0.19
	Spring 2016	122	50–150	36.1 ± 0.2	14.8 ± 1.0	26.3 ± 18.3	8.00 ± 0.03	2319 ± 17	2117 ± 19	10.64 ± 0.06	2.21 ± 0.18
	Summer 2016	129	30–90	36.2 ± 0.2	17.5 ± 2.2	6.8 ± 23.8	8.00 ± 0.05	2309 ± 15	2077 ± 25	10.60 ± 0.07	2.52 ± 0.31
	Autumn 2016	129	5–25	36.4 ± 0.1	18.4 ± 2.7	6.3 ± 19.6	7.99 ± 0.02	2329 ± 13	2101 ± 19	10.64 ± 0.06	2.50 ± 0.27
	Winter 2016	129	50–110	36.4 ± 0.1	18.1 ± 1.0	12.0 ± 10.8	8.02 ± 0.02	2333 ± 11	2088 ± 11	10.66 ± 0.05	2.64 ± 0.17
Intermediate (100–500 m)	Spring 2014	13		36.2 ± 0.5	13.6 ± 0.5	49.6 ± 9.4	8.01 ± 0.02	2292 ± 47	2088 ± 40	10.62 ± 0.15	2.17 ± 0.13
	Summer 2014	17		36.3 ± 0.5	14.2 ± 0.8	47.7 ± 13.7	7.95 ± 0.04	2294 ± 47	2111 ± 50	10.64 ± 0.15	2.00 ± 0.16
	Autumn 2014	15		36.2 ± 0.3	14.5 ± 0.5	44.9 ± 8.6	7.95 ± 0.05	2295 ± 34	2112 ± 44	10.62 ± 0.09	2.01 ± 0.23
	Winter 2014	14		36.4 ± 0.4	15.4 ± 0.8	39.1 ± 10.1	8.00 ± 0.03	2316 ± 53	2098 ± 47	10.69 ± 0.12	2.34 ± 0.20
	Spring 2015	16		36.1 ± 0.3	13.6 ± 0.7	32.6 ± 17.6	8.03 ± 0.08	2323 ± 36	2106 ± 41	10.58 ± 0.09	2.33 ± 0.41
	Summer 2015	15		36.2 ± 0.4	14.4 ± 0.8	43.1 ± 16.3	7.98 ± 0.04	2325 ± 38	2121 ± 39	10.63 ± 0.12	2.18 ± 0.20
	Autumn 2015	15		36.1 ± 0.4	13.7 ± 0.5	51.3 ± 7.9	7.88 ± 0.04	2321 ± 50	2170 ± 44	10.59 ± 0.11	1.74 ± 0.17
	Winter 2015	14		36.4 ± 0.4	15.0 ± 0.6	43.1 ± 9.8	8.00 ± 0.01	2316 ± 30	2105 ± 29	10.68 ± 0.11	2.27 ± 0.10
	Spring 2016	60		36.1 ± 0.5	13.9 ± 1.1	53.9 ± 22.6	7.94 ± 0.04	2318 ± 38	2139 ± 37	10.62 ± 0.15	2.00 ± 0.21
	Summer 2016	53		36.2 ± 0.5	13.8 ± 1.0	53.3 ± 13.0	7.95 ± 0.04	2308 ± 49	2124 ± 41	10.60 ± 0.17	2.02 ± 0.18
	Autumn 2016	54		36.2 ± 0.5	13.7 ± 0.9	50.8 ± 11.7	7.94 ± 0.02	2318 ± 43	2142 ± 34	10.58 ± 0.15	1.95 ± 0.15
	Winter 2016	53		36.3 ± 0.5	14.7 ± 1.0	48.8 ± 15.6	7.97 ± 0.02	2328 ± 43	2132 ± 37	10.64 ± 0.16	2.15 ± 0.16
Deep (>500 m)	Spring 2016	10		36.8 ± 0.4	13.2 ± 0.5	73.9 ± 12.2	7.92 ± 0.03	2366 ± 45	2188 ± 43	10.84 ± 0.15	1.97 ± 0.10
	Summer 2016	10		36.6 ± 0.4	13.2 ± 0.5	66.2 ± 4.3	7.94 ± 0.02	2344 ± 36	2157 ± 26	10.74 ± 0.13	2.03 ± 0.12
	Autumn 2016	9		36.8 ± 0.4	13.3 ± 0.3	62.6 ± 2.8	7.93 ± 0.01	2368 ± 32	2186 ± 24	10.78 ± 0.12	2.00 ± 0.09
	Winter 2016	8		36.8 ± 0.5	13.8 ± 0.5	70.1 ± 11.8	7.95 ± 0.02	2377 ± 42	2185 ± 31	10.81 ± 0.15	2.10 ± 0.15

2.5. Statistical analysis

The principal descriptive statistics (mean, standard deviation, minimum and maximum values) were determined in the dataset. For analysing differences on hydrological and biogeochemical characteristics the one-way analysis of variance test (ANOVA) was used. The threshold values for statistical significance were taken as $p < 0.05$. These statistical analyses were performed with IBM SPSS Statistics software (version 20.0; Armonk, New York, USA). Linear correlations and figures were carried out using SigmaPlot software version 11.0, and Figs. 3, 6, S4 and S5 were performed with Ocean Data View. Moreover, the uncertainties of the different linear equations were calculated through the reproducibility of the analytical measurements.

3. Results

3.1. Vertical distribution

Table 1 presents the average values of the hydrological and biogeochemical characteristics studied for the cruises followed between the years 2014 and 2016, including three vertical depth ranges according to the presence of the water mass majority. Therefore, they were differentiated in surface, intermediate and deep intervals, although this last water mass was only registered during the 2016 cruises (only one station was deeper than 500 m in STOCA cruises). S_P values showed a variability between 35.2 and 37.8, being the highest mean values recorded in deep waters (36.8 ± 0.4) (Table 1), and the values among surface and intermediate depths did not present significant differences. The mean T values were similar for intermediate and deep depths (14.1 ± 1.0 and 13.4 ± 1.0 °C, respectively), but significantly different to surface values that presented the highest mean T values (17.2 ± 1.6 °C). Some anomalies were detected in these surface waters, due to the fact that the cruises were carried out from the beginning of each meteorological season (Table 1), showing the highest average T values during winter (18.1 ± 1.3 °C) and the lowest in spring (14.8 ± 0.8 °C). AOU mean values presented significant differences between the three depth ranges and varied from −55.0 to 106.3 μmol kg^{-1}. An increase towards the deepest waters was observed, reaching a mean AOU value of 66.5 ± 10.4 μmol kg^{-1} (Table 1) derived from the decrease of the photosynthetic activity and a greater influence of the respiration processes (Fig. 2). However, pH_T values displayed a slight depletion with depth (Fig. 2), and were only significantly different to the surface depth, which presented the highest mean values (8.01 ± 0.05) (Table 1). TA and DIC presented a similar behaviour with depth, hence the vertical profile for TA is the only one represented (Fig. 2). The mean values of TA and DIC were of 2363 ± 41 and 2175 ± 38 μmol kg^{-1}, respectively, with a weak increase in deep waters for both variables (Table 2). These values are similar to those measured by other authors in the GoC (Santana-Casiano et al., 2002; Ribas-Ribas et al., 2011; Flecha et al., 2012, 2019). Although there is no vertical variation of [Ca^{2+}] in Fig. 2, Table 1 reflects the slightly increase of these concentrations in deeper waters up to 10.81 ± 0.13 mmol kg^{-1}. In fact, the mean Ca^{2+} values only presented significant differences with the deep waters. The study area was supersaturated of $CaCO_3$ in all the water column (Fig. 2) and during all the cruises (Table 1). Thus, ΩAr ranged from 1.42 to 3.72, with similar values in intermediate and deep waters (Table 1) and being significantly different with the surface water values. A high variability was also observed in this surface layer (Fig. 2), due to the intense biological activity and continental inputs from the rivers in the area, which are composed of carbonated nature basins.

3.2. Surface seasonal variation

The seasonal variation of the studied variables in this work has been determined in the shallowest waters (Table 2), an area considered as highly variable due to some factors, such as, the constant interaction

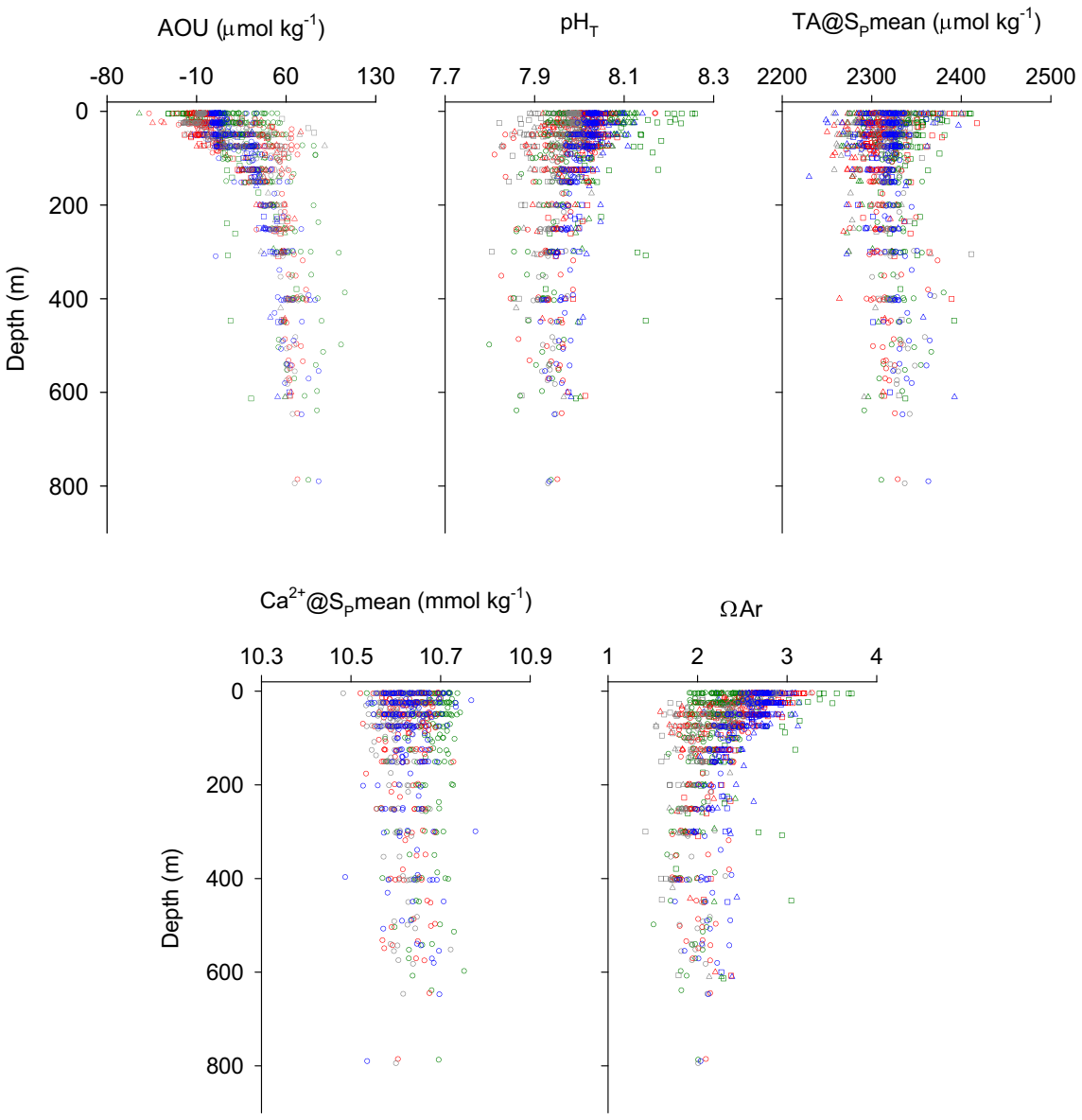

Fig. 2. Vertical profiles of apparent oxygen utilization (AOU), pH_T (pH at in situ temperature), total alkalinity and calcium concentration normalized to the mean salinity (36.26) of the sampling period (TA@$S_P$mean and Ca^{2+}@$S_P$mean, respectively), and aragonite saturation state (ΩAr) measured in the fixed sampling stations during the years 2014 (triangle), 2015 (square) and 2016 (dot), as well as the different cruises completed in spring (green), summer (red), autumn (grey), and winter (blue).

Table 2
Number of samples (n), mean values and standard deviations of practical salinity (S_P), temperature (T), apparent oxygen utilization (AOU), pH_T (pH at in situ temperature), total alkalinity (TA), dissolved inorganic carbon (DIC), calcium concentration (Ca^{2+}), and aragonite saturation state (ΩAr) measured in surface waters (~5 m) at fixed stations, for the different cruises followed between 2014 and 2016.

Cruise	n	S_P	T (°C)	AOU (μmol kg^{-1})	pH_T	TA (μmol kg^{-1})	DIC (μmol kg^{-1})	Ca^{2+} (mmol kg^{-1})	ΩAr
Spring 2014	16	36.1 ± 0.1	15.2 ± 0.5	−4.3 ± 15.4	8.09 ± 0.03	2289 ± 11	2049 ± 32	10.58 ± 0.04	2.65 ± 0.14
Summer 2014	16	36.2 ± 0.1	20.8 ± 1.4	−10.2 ± 5.7	7.99 ± 0.04	2308 ± 25	2069 ± 31	10.62 ± 0.03	2.69 ± 0.18
Autumn 2014	16	36.1 ± 0.1	21.5 ± 0.7	−4.3 ± 3.2	7.99 ± 0.05	2307 ± 42	2060 ± 32	10.58 ± 0.03	2.76 ± 0.28
Winter 2014	16	36.2 ± 0.3	17.6 ± 0.7	8.0 ± 2.1	8.06 ± 0.04	2326 ± 31	2068 ± 42	10.65 ± 0.03	2.59 ± 0.73
Spring 2015	16	36.0 ± 0.1	15.4 ± 0.3	−18.8 ± 9.4	8.12 ± 0.12	2338 ± 37	2067 ± 56	10.57 ± 0.04	2.93 ± 0.67
Summer 2015	16	36.4 ± 0.1	21.0 ± 0.9	−2.2 ± 3.2	8.03 ± 0.03	2365 ± 27	2088 ± 23	10.68 ± 0.01	2.95 ± 0.16
Autumn 2015	16	36.2 ± 0.1	20.5 ± 1.2	−1.9 ± 5.0	7.96 ± 0.03	2347 ± 41	2118 ± 33	10.62 ± 0.01	2.88 ± 0.06
Winter 2015	16	36.5 ± 0.1	20.5 ± 0.3	0.3 ± 1.6	8.03 ± 0.01	2318 ± 7	2051 ± 11	10.69 ± 0.02	2.81 ± 0.07
Spring 2016	37	36.2 ± 0.2	14.8 ± 1.1	20.9 ± 16.3	7.99 ± 0.04	2320 ± 18	2116 ± 21	10.64 ± 0.05	2.24 ± 0.18
Summer 2016	37	36.2 ± 0.2	19.6 ± 1.3	−7.8 ± 9.3	8.03 ± 0.04	2314 ± 12	2060 ± 24	10.60 ± 0.07	2.77 ± 0.14
Autumn 2016	37	36.5 ± 0.1	21.6 ± 1.0	−5.6 ± 2.2	7.99 ± 0.01	2338 ± 9	2087 ± 17	10.68 ± 0.05	2.78 ± 0.09
Winter 2016	37	36.4 ± 0.1	18.5 ± 0.7	7.1 ± 7.0	8.03 ± 0.01	2335 ± 11	2082 ± 14	10.67 ± 0.05	2.72 ± 0.09

with the atmosphere, the biological activity, the influence of the continental inputs and the mixing processes. The S_P values presented significant differences for each season, although they showed a low variability (Table 2), with a mean value of 36.3 ± 0.2 for the whole study. The range of variation observed for T values was higher, from 13.1 to 22.9 °C, without significant differences, except for the seasons of spring. Moreover, the highest average values obtained were during autumn (21.3 ± 1.1 °C) and the lowest occurred in spring (15.0 ± 0.9 °C), since they were measured at the beginning of each season. AOU values in each season presented significant differences and followed a seasonal variation with negative average values during summer and autumn (−7.7 ± 8.0 and −4.7 ± 3.6 μmol kg^{-1}, respectively) due to the greater photosynthetic activity, and positive values in spring and winter (5.3 ± 22.8 and 5.9 ± 6.1 μmol kg^{-1}, respectively). Although during the spring cruises, the mean values obtained in 2015 and 2016 were the minimum (−19.3 ± 9.4 μmol kg^{-1}) as well as the maximum (21.1 ± 16.3 μmol kg^{-1}) recorded for the complete study, possibly due to the storm conditions in the latter case, which lead to an increasing of the mixing processes (Table 2). pH_T mean values did not show much difference between the different cruises followed in this study (8.02 ± 0.06). However, they presented significant differences for each season, with the highest values in spring and winter, and the lowest in summer and autumn, according to temperature variation (Table 2). Surface waters also showed a high variability of TA and DIC, with a variation range of 2244 to 2466 μmol kg^{-1}, and 1935 to 2171 μmol kg^{-1}, respectively. The mean values for both variables did not follow a constant variation between seasons during the whole study (Table 2). The variation of $[Ca^{2+}]$ was between 10.45 and 10.81 mmol kg^{-1} (Table 2), with a mean value, for each season, close to the total average value (10.64 ± 0.06 μmol kg^{-1}). ΩAr values showed greater variations in surface waters (1.91–3.72) (Fig. 2). The ΩAr mean value (2.68 ± 0.28) is located in the lower part of the range variation described by Jiang et al. (2015) for North Atlantic surface waters (2.36–3.95) at latitudes between 30°N and 50°N where the GoC is located (Fig. 1). ΩAr presented seasonal significant differences, with the lowest mean value obtained during spring (2.61 ± 0.35), and the highest in summer (2.80 ± 0.13) due to the greater photosynthetic activity in this season.

4. Discussion

4.1. Variation in the surface mixed layer in the GoC

The SML usually constitutes the top 20–100 m of the water column located above the thermocline (Thompson, 1976). It is the most reactive zone within the water column due to its higher water temperature and exposure to sunlight, which allows processes as photosynthesis, lower hydrostatic pressure, and the exchange of gases with the atmosphere (Dinauer and Mucci, 2018). Another process to consider in the SML is the oxidation of organic matter in the areas close to the thermocline depth, which produces low values of DO and an important effect over the carbonate system. The depth range of SML in the GoC has been established in the first 100 m of the water column, this includes the upper limit of the thermocline depths determined for this study period (5–125 m) (Sierra et al., 2017; Amaral et al., 2020).

Fig. 3 presents the pH_T, TA and ΩAr mean values distribution for the complete study in the SML at three different depths: surface waters (~5 m), in the maximum of Chl concentrations and in the maximum of AOU values (31.3 ± 21.9 m and 48.0 ± 29.3 m, respectively). It can be observed how these variables change depending on depth. pH_T in surface waters present the highest values, with an average of 8.03 ± 0.05, which could be due to the fact that the surface partial pressure of CO_2 (pCO_2) is near to the balance with the atmosphere. In this respect, Jiménez-López et al. (2019) described that the eastern shelf of the GoC acted weakly as a sink of CO_2 (−0.18 ± 1.32 mmol m^{-2} d^{-1}) between 2014 and 2015, which showed to be near to an equilibrium with the atmosphere. The relatively high pH_T values were observed in the maximum Chl depth accompanied by a decrease in the maximum AOU depth because of the organic matter degradation processes. This pH_T change influences on $[CO_3^{2-}]$ resulting in a progressive decrease of TA and ΩAr with depth in the SML (Fig. 3).

In general, TA and ΩAr presented the highest values in the offshore waters (Fig. 3) related to the presence of the eastward branch of the Azores Current that introduces warmer waters in this part of the GoC (Gould, 1985; Käse et al., 1985; Johnson and Stevens, 2000). Jiménez-López et al. (2019) also found that the temperature and pCO_2 values in the surface waters of the GoC were higher in these offshore areas influenced by this branch. In those areas near to the Moroccan coast and the external stations of TF, lower values of pH_T and ΩAr, and higher of TA were observed (Fig. 3), which may be due to the existing upwelling along the African coast of the Strait of Gibraltar (Stanichny et al., 2005). By contrast, the lowest pH_T, TA and ΩAr values were observed in the central area of the studied region, mainly in the depths matching the maximum AOU values (Fig. 3). In this area, the stability of the thermocline depth is greater, since it is weakly influenced by the surface coastal currents of the GoC and the eastward branch of the Azores.

Additionally, pH_T, TA and ΩAr showed a higher variability in the coastal area (Fig. 3). In this regard, the waters near to the Guadiana estuary displayed high values of pH_T and ΩAr, and moderately high values of TA, probably derived from the drift of the filament off Cape St. Vincent (Relvas and Barton, 2002; Criado-Aldeanueva et al., 2006). Moreover, in this area is where the highest Chl concentrations were found for the whole study (González-García et al., submitted), which could explain a major primary productivity and therefore higher pH_T and ΩAr. In the coastal area of TF, there is an upwelling as a result of the tidal-topographical interaction that produces an increase of the primary production in the zone (e.g. Prieto et al., 1999; Vargas-Yáñez et al., 2002) and it can be observed in Fig. 3 by a relative increase of pH_T, TA and ΩAr. Finally, it can also be appreciated a certain increase of pH_T and ΩAr in the coastal areas near to the Guadalquivir estuary mouth. It should be pointed out that the GoC receives significant contributions from the rivers located in this basin, being the Guadalquivir River responsible for about 90% of the freshwater discharges to its close onshore waters (González-Ortegón and Drake, 2012). In this respect, Fig. 4 presents the evolution of TA, DIC and $[Ca^{2+}]$ with S_P in the Guadalquivir estuary for the five samplings carried out between July 2017 and April 2019. The relationships observed for these variables with S_P indicate that the inner parts of this estuary are related with high TA, DIC and $[Ca^{2+}]$, therefore resulting in an considerable input towards the GoC. If we consider the average flow of the Guadalquivir River, between 2017 and 2019 (48.6 m^3 s^{-1}, Confederación Hidrográfica del Guadalquivir, España, n.d.; http://www.chguadalquivir.es/saih/DatosHistoricos.aspx), in addition to the TA, DIC and $[Ca^{2+}]$ values in the river end member, we can conclude that the estuary provided 6.2 Gmol yr^{-1} of TA and DIC, and 4.0 Gmol yr^{-1} of Ca^{2+} to the close coastal areas. Under these conditions, there would be an increase of 1.4 μmol kg^{-1} d^{-1} of TA and DIC, and 0.8 μmol kg^{-1} d^{-1} of Ca^{2+} in the 400 km^2 around the Guadalquivir estuary mouth. According to this estimation, Hu et al. (2017) determined that the coastal waters affected by rivers with high levels of weathering products ($CaCO_3$ river basin) represent well-buffered systems.

Other studies also consider that the variation of ΩAr in surface waters is mainly controlled by biological processes (primary production and aerobic respiration principally), temperature and mixing processes (Cai et al., 2011; Jiang et al., 2015; Xue et al., 2017). If ΩAr changes are decomposed into different processes in the SML (Xue et al., 2017), the primary process controlling seasonal ΩAr net change is the biological activity (Fig. S1), while gas exchange and mixing only play important roles during some seasons in this interannual study in the GoC. The absolute value of the relative importance of in situ biological activity process is always greater than 35%, and produces a change in ΩAr between −0.41 in winter 2015 and 0.52 in autumn 2015. With the exception of winter 2014, under storm conditions, the relative importance of

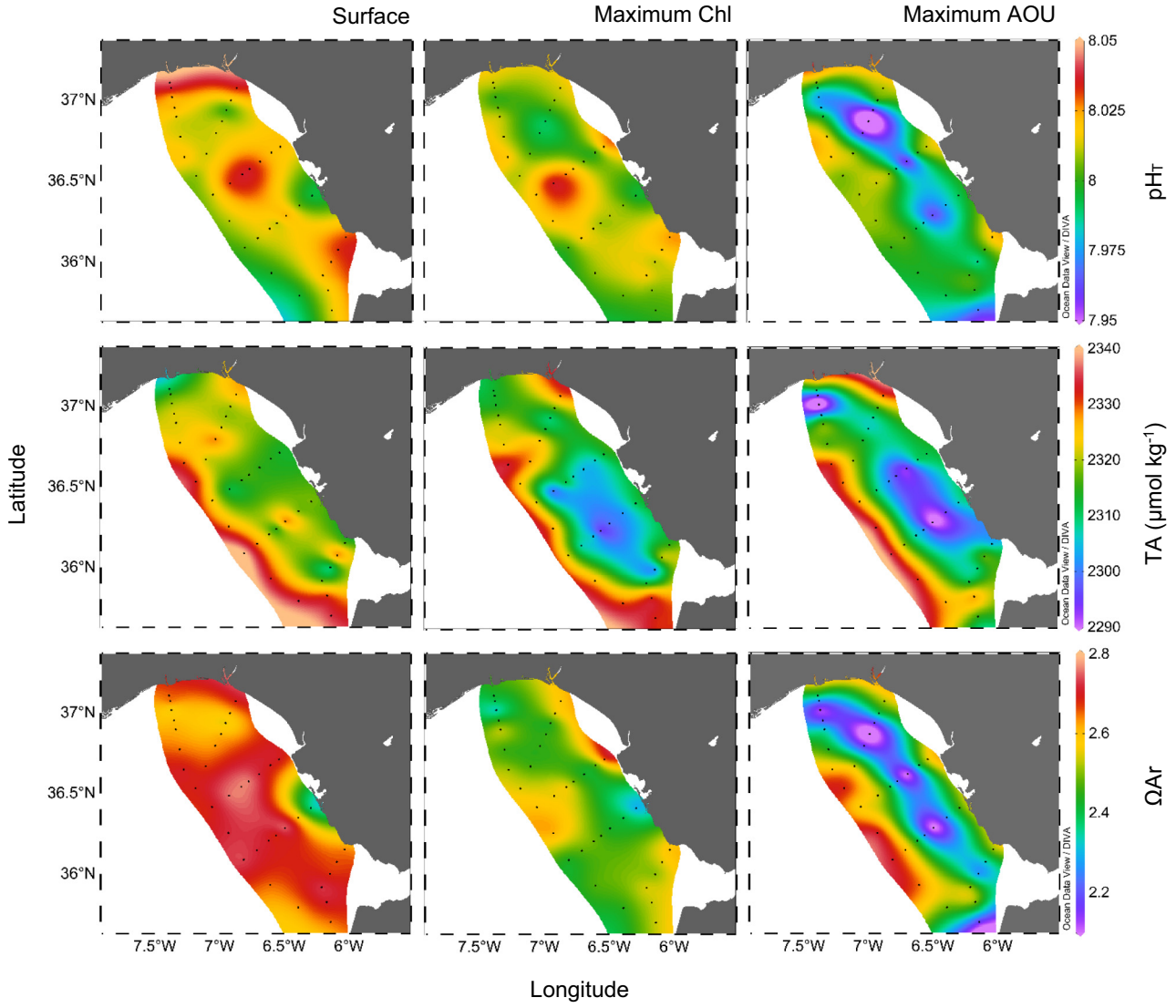

Fig. 3. Spatial distribution of mean values of pH_T (pH at in situ temperature), total alkalinity (TA) and aragonite saturation state (ΩAr) between the years 2014 and 2016 at different depths: surface (~5 m), in the maximum chlorophyll a concentrations (Chl) and in the maximum apparent oxygen utilization values (AOU).

temperature, exchange with the atmosphere and mixing processes in ΩAr variability are usually lower than ±10%. There is a good linear relationship between the contributions of individual processes to changes in ΩAr in the coastal and distal areas (Fig. S2), with a greater importance of these processes in the variability of ΩAr in the coastal zone. In this respect, the effects of temperature and biological activity on ΩAr in the distal area affect a 15% lower than in the coastal area. The coastal region of the GoC has a greater thermal variability (Jiménez-López et al., 2019) and higher concentrations of nutrients and Chl (González-García et al., 2018). The contributions of the mixing processes is a 35% lower in the distal zone, related to the greater importance of the continental inputs and upwelling effects in the coastal area, mainly produced by the drift of the filament off Cape St. Vincent and the upwelling of TF (Relvas and Barton, 2002; Vargas-Yáñez et al., 2002). The influence of sea-air CO_2 exchange on ΩAr variations is more than a 50% lower in the distal zone. Jiménez-López et al. (2019) describes how the sea-air CO_2 fluxes vary with the distance to coast in the GoC, and they are higher and more variable in the coastal region.

Moreover, our study area showed that ΩAr was negatively correlated with AOU and NO_3^- in the SML (Fig. 5), which supports the hypothesis that biological activity is the main process that controls changes in ΩAr. The primary productivity leads to the uptake of CO_2, rising the pH values in the water and consequently causing an increase of $[CO_3^{2-}]$ and ΩAr. Previous studies in coastal areas have shown that the existence of a high production in surface waters can make the pH, DO and ΩAr concentrations grow (Xue et al., 2016; Hu et al., 2017; Cai et al., 2017; Cotovicz et al., 2018; Li et al., 2020). Also, in the SML, a ΩAr rate of 0.089 $°C^{-1}$ was obtained, which is close to the one determined in the surface waters of the Atlantic Ocean ($z < 100$ m) by Jiang et al. (2015) (0.086 $°C^{-1}$). This trend could be attributed to the T influence in the inorganic carbonate equilibrium (carbonate equilibrium constants) and the aragonite solubility product. When the water T increases, the first and second carbon dissociation constants increase, resulting in an increase of $[CO_3^{2-}]$ and ΩAr, and a decrease of the aragonite solubility product (Dickson and Millero, 1987).

Finally, the buffer factor changes in the CO_2 system in the SML have been calculated in order to have a better understanding of the buffer capacity in the GoC waters (Table S1). The buffer factors present average values for the studied area of 0.19 ± 0.01, 0.23 ± 0.01 and −0.27 ± 0.02 for γ_{DIC}, β_{DIC} and ω_{DIC}, respectively, and R value of 10.9 ± 0.5. If we compare these data with those of the entire global surface ocean of 1994 presented by Egleston et al. (2010), we observe that they are within the range shown in the Atlantic Ocean and we could conclude that the GoC is a well buffered system. In fact, the values of the buffer factors and R calculated are very similar to those obtained by Álvarez et al. (2014) in the GoC. Furthermore, significant differences in γ_{DIC}

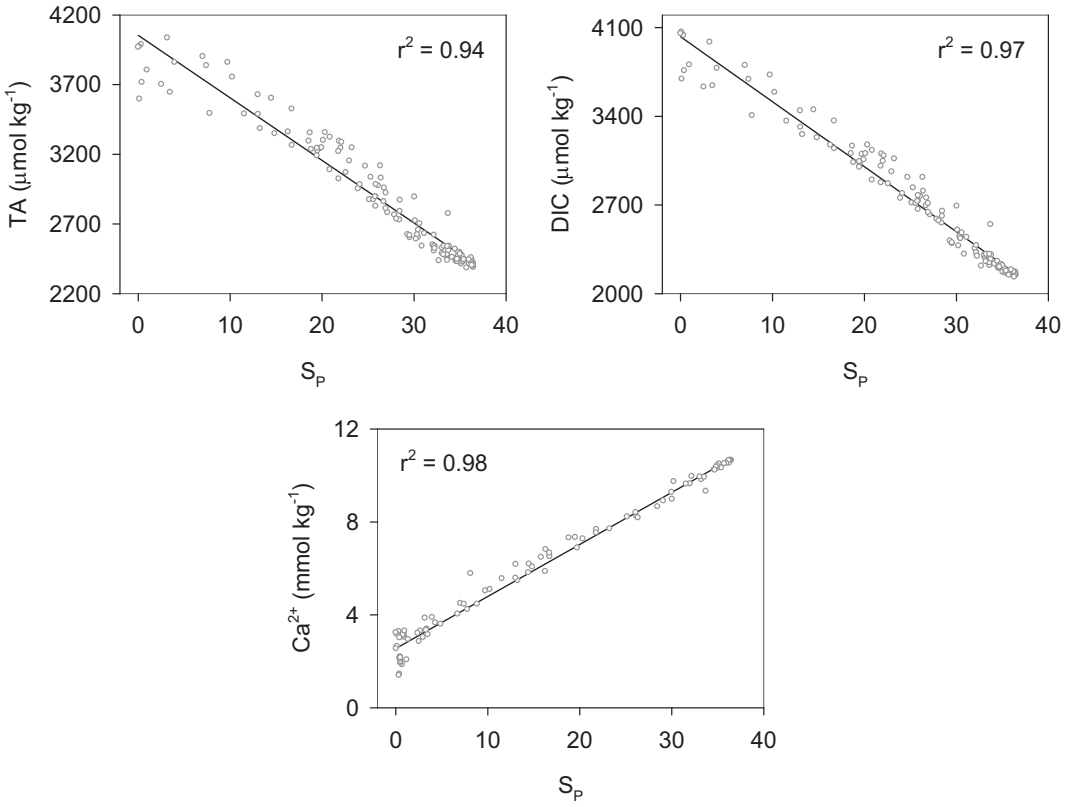

Fig. 4. Correlation between the measured values of total alkalinity (TA), dissolved inorganic carbon (DIC) and calcium concentration (Ca^{2+}) with practical salinity (S_P) (TA = 4053 (±1) − 44.85 (±0.03)·S_P, n = 129; DIC = 4027 (±1) − 51.26 (±0.03)·S_P, n = 129; Ca^{2+} = 2.55 (±0.46) + 0.224 (±0.022)·S_P, n = 98, respectively) for the different cruises between the years 2017 and 2019 in the Guadalquivir estuary.

and β_{DIC} have been found between the coastal and distal areas. Therefore, the CO_2 and $[H^+]$ dissolved in the coastal waters seem to be slightly less sensitive to changes in DIC than in the distal waters. However, ω_{DIC} did not present spatial differences in the study area, so the carbonate saturation state (or $[CO_3^{2-}]$) has the same ability to resist changes in DIC in the coastal and distal zones of GoC. By examining the R value, we can conclude that for a given change in CO_2 the relative change in DIC for coastal waters is lower than in distal waters.

In other coastal systems, intervals of variation of the buffer factors have been found to be quite similar to those obtained in the GoC (Hu et al., 2017; Cotovicz et al., 2018; Urbini et al., 2020). In these systems, the high buffer capacity is attributed to different reasons, including the high surface primary productivity, the relatively warm waters and the presence of highly buffered river water (high TA). Fig. S3 presents the relationship between the buffer factors calculated in the GoC with TA/DIC ratio, AOU, and T. It shows as the biological activity and T influence on the variability of these factors. The lowest AOU values in addition to the highest TA/DIC and T values were related to the highest buffer capacity in the SML of the GoC, which was probably due to the primary productivity that increases the TA/DIC ratio and decreases the AOU. Additionally, the increase of T produces shifts in acid-base dissociation constants and a consequent rise of the buffering capacity (Urbini et al., 2020).

4.2. Variation in deep waters ($z > 100$ m)

The distribution of the different water masses in the GoC determines the variations of Ca^{2+} and ΩAr found in the deep waters (z > 100 m), with the presence of two major masses, NACW ($NACW_T$ and $NACW_P$) and MOW (Fig. 6). But despite the existence of a particular stratification of these water masses, the study area registers important mixing processes that alter their characteristics. A break of the depth thermocline influenced by storm events during spring 2016 (e.g. González-Dávila et al., 2003), a decrease of S_P values due to freshwater discharges (van Geen et al., 1991), and/or the presence of upwelling events induced by the topography of the zone and the wind (Criado-Aldeanueva et al., 2009; Peliz et al., 2009) could affect the NACW thermohaline properties. Additionally, there is a mixture between NACW and the surface waters in the coastal area by the interaction with the bottom, and with MOW that flows along with the topography in the deeper waters (Hernández-Molina et al., 2014).

TA and $[Ca^{2+}]$ showed a practically conservative behaviour in deep waters (Fig. 7), which indicates that the mixing processes among the different water masses is the main factor to establish their distributions, and the $CaCO_3$ precipitation is very weak in our study region. The lineal relationship between TA and S_P (TA = −761 (±13) + 85.73 (±0.35)·S_P, r^2 = 0.97, n = 256) is similar to others found in the GoC (Santana-Casiano et al., 2002; Aït-Ameur and Goyet, 2006; Huertas et al., 2009; Flecha et al., 2012). However, there are no previous experimental measurements of Ca^{2+} in this study area and the relationship observed ($[Ca^{2+}]$ = 293.3 (±0.4)·S_P, r^2 = 0.93, n = 256) is similar to the one obtained by Culkin and Cox (1966) ($[Ca^{2+}] = 293.6 \cdot S_P$). Furthermore, Rosón et al. (2016) found a lower relationship based in the experimental measurement of a larger collection of samples in the subtropical Atlantic Ocean ($[Ca^{2+}] = 292.5 \cdot S_P$). These authors calculated an overestimation in the quantification of ΩAr (0.5 ± 0.2%) when using measured $[Ca^{2+}]$ from S_P values based on overall the relationship of Culkin and Cox (1966). The relationship between $[Ca^{2+}]$ and S_P was expected to be lower in the GoC, since NACW is the more abundant water mass and has low S_P values. The differences found with Rosón et al. (2016) may be due to the $[Ca^{2+}]$ variations associated with the presence of the Mediterranean water that presents a higher $[Ca^{2+}]$

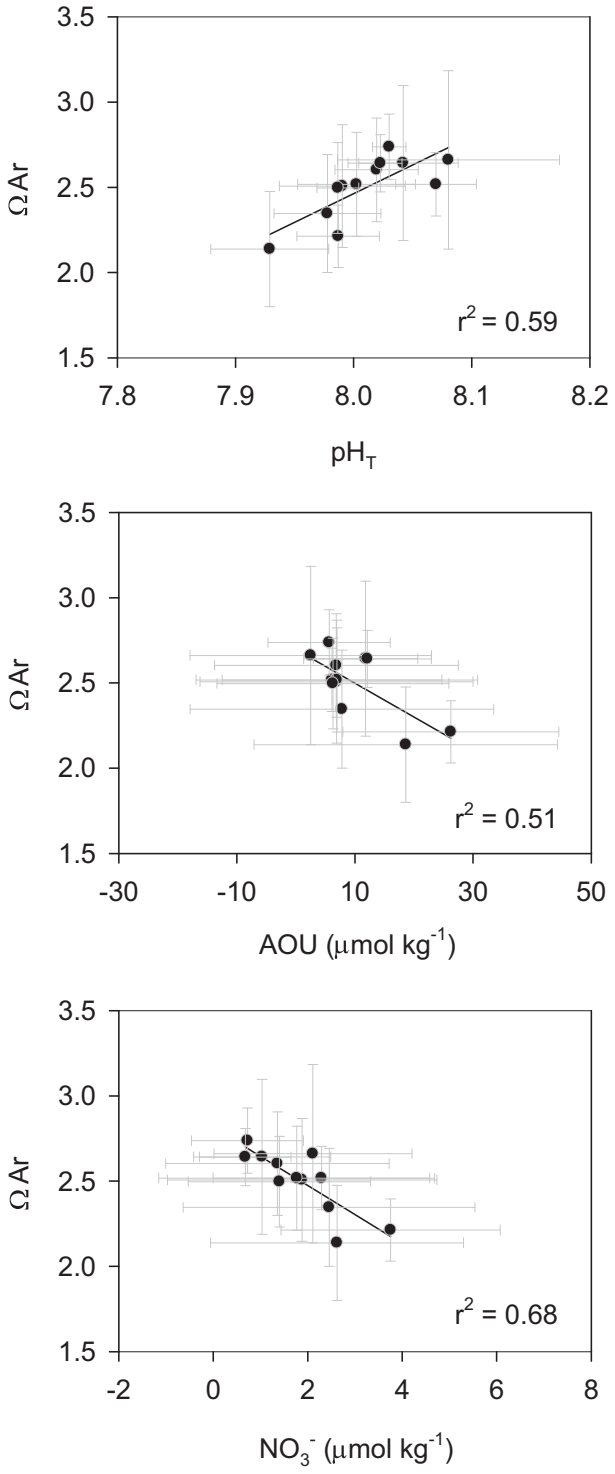

Fig. 5. Correlations between the mean values of aragonite saturation state (ΩAr) with pH$_T$ (pH at in situ temperature), apparent oxygen utilization (AOU) and nitrate concentration (NO_3^-) in the surface mixed layer (z < 100 m), for each sampling cruise (n = 12). Standard deviations are superimposed.

([Ca^{2+}] = 294.3·S_P, Culkin and Cox (1966)), the continental inputs in addition to the $CaCO_3$ dissolution in the surface sediments of the coastal area (Ferrón et al., 2009).

In general, the deep waters in the studied area of the GoC present a 40.3% of NACW$_T$, a 47.8% of NACW$_P$ and an 11.9% of MOW. Fig. 6 shows the mean annual variations during 2016 cruises of the distribution of the different water masses identified in TF, SP, GD, TO and GU transects below the SML. NACW$_T$ (T = 17.3 °C, S_P = 36.50, Flecha et al., 2012) is located under the thermocline depth, with an important contribution to depths close to 100 m and it represents the most abundant water mass up to 200 m. Below, NACW$_P$ (T = 11.3 °C, S_P = 35.55, Flecha et al., 2012) is placed between 200 and 500 m, with a higher presence around 400 m, and towards the coastal area this water mass acquires a greater importance towards lower depths (>40% for 100–200 m). Finally, MOW (T = 13.1 °C, S_P = 38.50, Flecha et al., 2012) is detected near the bottom, at depths deeper than 500 m, and its contribution decreases towards the west, from approximately 40% in the SP transect to less than a 20% in GU transect. In the TF transect this is the major water mass for depths over 300 m (>60%). Additionally, Figs. S4 and S5 (Supplementary material) show the mean annual variations below the SML of T, S_P, AOU, NO_3^-, pH, TA, Ca^{2+} and ΩAr in the TF, SP, GD, TO and GU transects during the 2016 cruises.

Table 3 presents the concentrations of Ca^{2+}, TA, ΩAr, pH$_T$ and AOU estimated for NACW$_T$, NACW$_P$ and MOW. The vertical variations of [Ca^{2+}] and TA are controlled by changes in S_P, with relatively high values at about 100 m deep associated to NACW$_T$ (10.69 ± 0.09 mmol kg^{-1}, 2357 ± 10 µmol kg^{-1}, respectively), showing a progressive decrease at about 400 m where the NACW$_P$ signal is maximum (10.41 ± 0.09 mmol kg^{-1}, 2303 ± 10 µmol kg^{-1}, respectively), and resulting with the highest values in the deeper waters due to the presence of MOW (11.32 ± 0.12 mmol kg^{-1}, 2465 ± 9 µmol kg^{-1}, respectively). On the contrary, the vertical variation of ΩAr does not show a conservative behaviour and it is more related to pH$_T$ (r^2 = 0.51, n = 256) than S_P (r^2 = 0.37, n = 256). In this regard, NACW$_P$ shows higher and lower AOU and pH$_T$ values than NACW$_T$, respectively (Table 3), probably due to the organic matter mineralization processes of the African coast, related with the northwest African upwelling system (Pérez et al., 2001). In the deepest area, the greatest AOU values are identified associated to the MOW characteristics (82.0 ± 4.0 µmol kg^{-1}), similar to those found by other authors (e.g. de la Paz et al., 2008), which have been attributed to accumulated organic matter mineralization in the Mediterranean basin (Huertas et al., 2009). Although, it is important to mention that there is a pH$_T$ increase in the deep zone with respect to NACW$_P$, due to the presence of MOW (e.g. Santana-Casiano et al., 2002). The Mediterranean Sea shows high values of pH$_T$ (e.g. Millero, 1979) and TA, associated to the influences from the inputs across the Black Sea, as well as the river discharges that affect the inorganic carbonate system (Aït-Ameur and Goyet, 2006). Due to the lower variability of [Ca^{2+}], ΩAr is more affected by the [CO_3^{2-}] changes, since it is very sensitive to pH variations. Thus, ΩAr ranges from 2.51 ± 0.07 at about 100 m deep (NACW$_T$) to its lowest value of 1.56 ± 0.06 at about 400 m (NACW$_P$), and finally increases again in the deep zone as a function of the MOW ratio (2.22 ± 0.06).

4.3. ΩAr decadal trend in the GoC

The coastal ocean has been highlighted in the last decade as an area where there is a large variability of the total carbonate system (Andersson and MacKenzie, 2012; Johnson et al., 2013). They are not only affected by the increase of the atmospheric CO_2 levels, but also by the coupled effects of various processes, such as, temperature, continental inputs, organic matter degradation, biological and mixing processes, and the increased risk of human impacts (Cai et al., 2011; Tynan et al., 2014; Xue et al., 2017). Data collected in the GoC during the 2006–2016 decade were studied to estimate the temporal evolution of the carbonate system parameters in the shallowest waters, considering a water column lower than 100 m, located between the Guadiana estuary and Cape Trafalgar. In this coastal zone, it is possible to compare our database with the one obtained by Ribas-Ribas et al. (2011) between 2006 and 2007.

Fig. 8 shows the decadal trend in the GoC of pH$_T$@Tmean and ΩAr@Tmean mean values for both surface (z < 20 m) and subsurface waters (z > 20 m). Both variables showed a similar decrease with time resulting in −0.0085 (r^2 = 0.91) and −0.0092 yr^{-1} (r^2 = 0.99) for

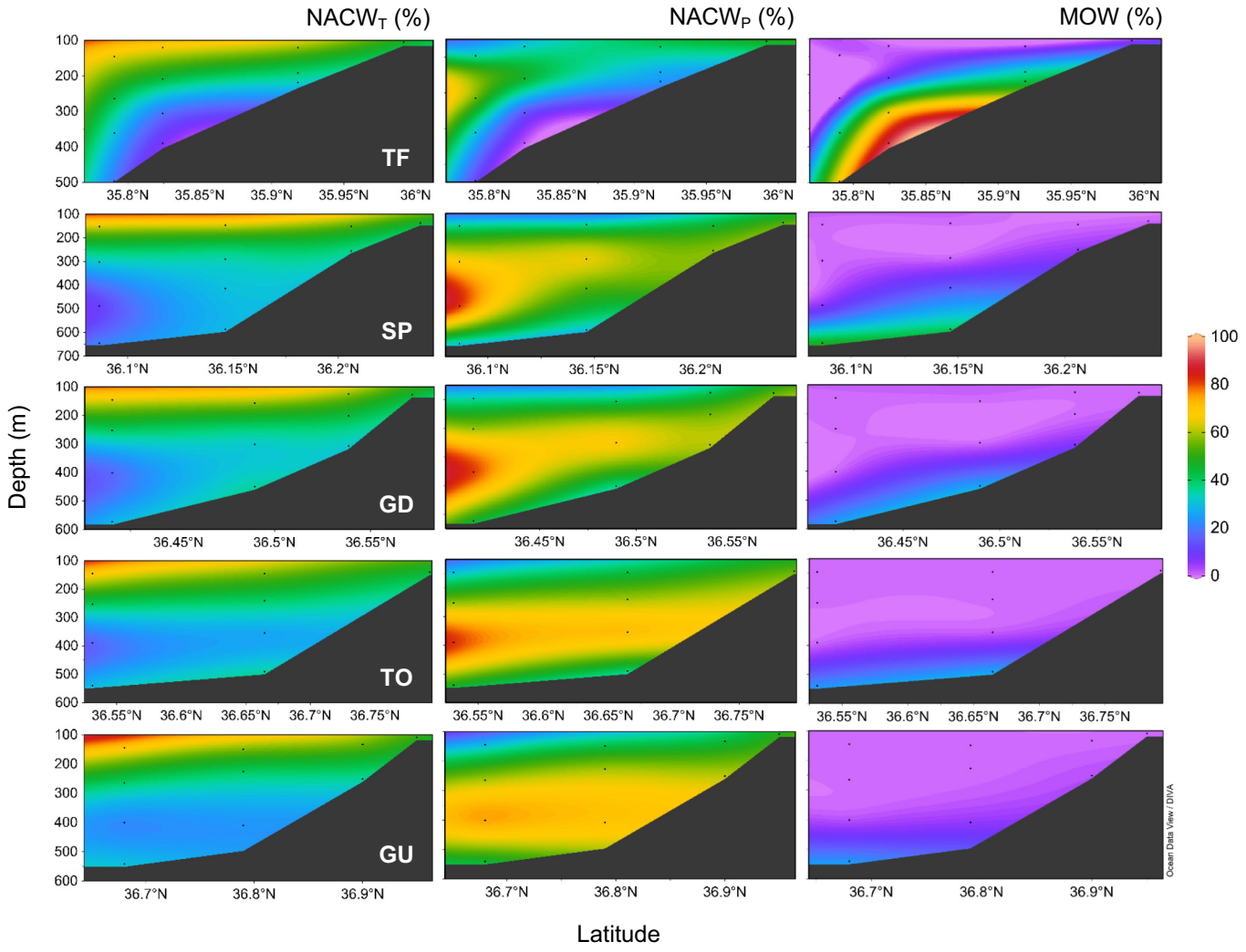

Fig. 6. Mean distribution of water masses (NACW$_T$, NACW$_P$ and MOW) obtained by the OMP analysis in the deep zone of the Gulf of Cádiz ($z > 100$ m), during 2016 for the different transects sampled: Trafalgar (TF), Sancti Petri (SP), Guadalquivir (GD), Tinto-Odiel (TO) and Guadiana (GU).

pH_T@Tmean, and −0.0554 ($r^2 = 0.93$) and −0.0550 yr^{-1} ($r^2 = 0.97$) for ΩAr@Tmean in surface and subsurface waters, respectively. These rates of pH decrease are within the range of variation found by Carstensen and Duarte (2019) in 83 coastal systems across the world (−0.023–0.023 yr^{-1}), and close to the value obtained by Borges and Gypens (2010) in the Belgian coast between 1990 and 1998 using R-MICO-CO_2 model (−0.006 yr^{-1}). Borges and Gypens (2010) also determined, in the same area, a ΩAr rate change near to the values obtained in this study (−0.047 ± 0.007 yr^{-1}). According to the pH and ΩAr variations obtained in this work, it seems that the GoC was subject to a

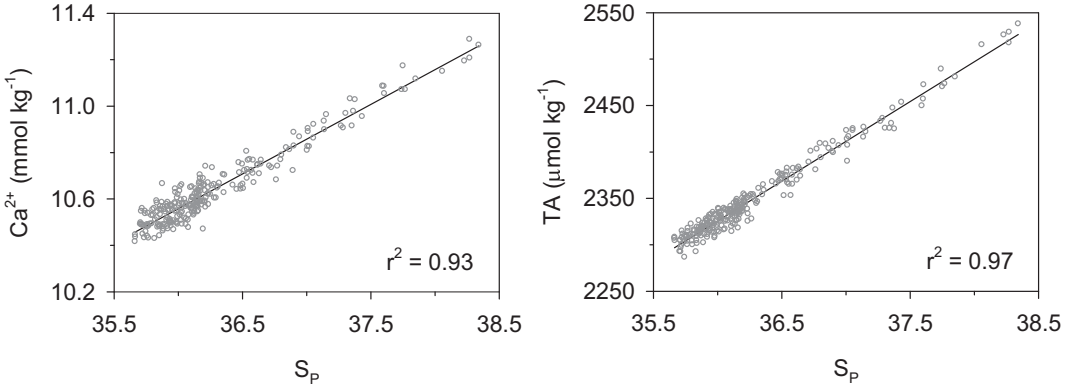

Fig. 7. Correlations between the measured values of calcium concentration (Ca^{2+}) and total alkalinity (TA) with practical salinity (S_P) ($Ca^{2+} = 293.3\ (\pm 0.4)\cdot S_P$; $TA = -761\ (\pm 13) + 85.73\ (\pm 0.35)\cdot S_P$, respectively) in the deeper water masses ($z > 100$ m) during the cruises realised in 2016 ($n = 256$).

Table 3
Mean values and standard deviations of calcium concentration (Ca^{2+}), total alkalinity (TA), aragonite saturation state (ΩAr), pH_T (pH at in situ temperature) and apparent oxygen utilization (AOU) associated to the different water masses ($NACW_T$, $NACW_P$ and MOW) during 2016 (n = 256).

	$NACW_T$	$NACW_P$	MOW
Ca^{2+} (mmol kg^{-1})	10.69 ± 0.09	10.41 ± 0.09	11.32 ± 0.12
TA (μmol kg^{-1})	2357 ± 10	2303 ± 10	2465 ± 9
ΩAr	2.51 ± 0.07	1.56 ± 0.06	2.22 ± 0.06
pH_T	8.00 ± 0.04	7.89 ± 0.05	7.97 ± 0.04
AOU (μmol kg^{-1})	21.7 ± 4.3	73.6 ± 2.9	82.0 ± 4.0

significative acidification trend over the 2006–2016 decade, which is strengthened with the acidification found by Flecha et al. (2019) in water masses exchanging through the Strait of Gibraltar. They determined an annual rate of pH, from 2005 to 2015, that varied between −0.0036 ± 0.0005 yr^{-1} and −0.0009 ± 0.0005 yr^{-1} for the NACW and the Western Mediterranean Deep Water, respectively. Furthermore, there is also some experimental evidence of acidification in the distal area of the GoC. Flecha et al. (2012) found mean values of spectrophotometric pH_T@25 of 8.00 ± 0.04, 7.92 ± 0.03 and 7.81 ± 0.04 in the SML, intermediate (100–500 m) and deep waters (>500 m) in a study carried out during October 2008. The pH_T@25 obtained in this work, for the same depth ranges, are relatively lower (7.91 ± 0.04, 7.80 ± 0.04 and 7.78 ± 0.04, respectively). However, the spatial differences in the areas studied, as well as the depth ranges and the lack of seasonal variations are enough factors to consider that the quantification of possible acidification using this database is not very adequate.

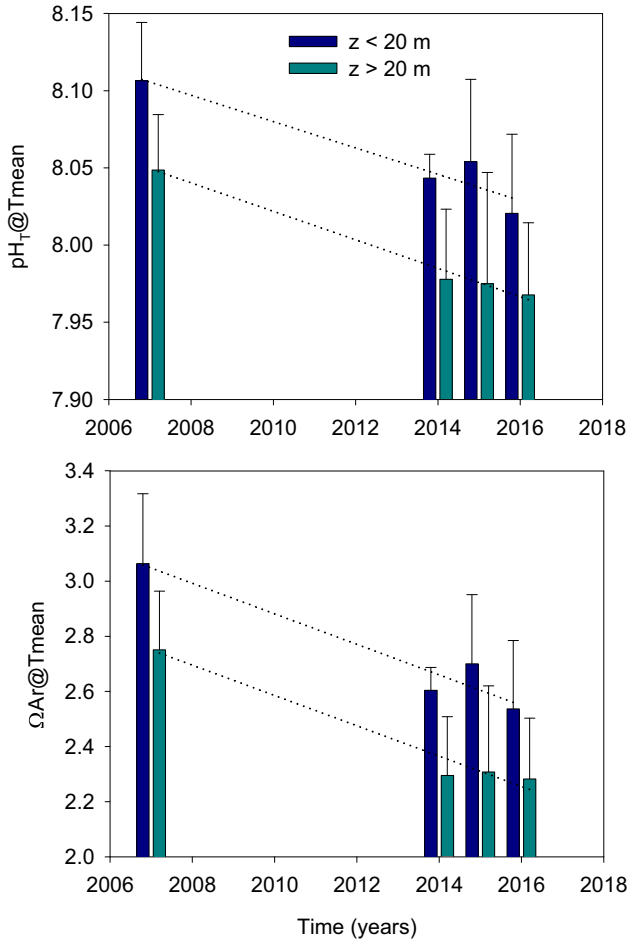

Fig. 8. Variation in the coastal area of the GoC (depth of the water column <100 m) of the normalized mean values of pH_T (pH_T@Tmean) and aragonite saturation state (ΩAr@Tmean) at the mean temperature (17.1 °C) registered for both databases used (Ribas-Ribas et al. (2011) and this study) between 2006 and 2016. The values are separated in two depth ranges: the upper water column (z < 20 m) and the lower water column (z > 20 m). Standard deviations area superimposed.

These decreases observed could be related to the constant increase of the atmospheric CO_2 concentration (~22.04 μatm between 2006 and 2016, Izaña Atmospheric Research Center in Spain - Earth System Research Laboratory; https://www.esrl.noaa.gov/gmd/dv/data/index.php) and the anthropogenic processes that have increased the coastal inputs of nutrients and carbon (e.g. Hofmann et al., 2011; Hu et al., 2018). If we assume this atmospheric CO_2 rise and consider the representative average values in surface waters for TA (2392 μmol kg^{-1}), S_P (36.2), and T (17.4 °C), this would lead to a pH and ΩAr changes of −0.0018 yr^{-1} and −0.012 yr^{-1}, respectively. But this pH and ΩAr decrease by year is lower than the estimated in coastal waters in the GoC (−0.0089 yr^{-1} and −0.0552 yr^{-1} on average, respectively). This difference suggests that pH and ΩAr in coastal areas of the GoC are also influenced by other processes, such as, biological activity, coastal inputs, in addition to mixed layer dynamics and not only by the atmospheric CO_2 uptake. In reference to the biological activity, the coastal zones are subjected to a strong decoupling of photosynthesis and respiration processes derived from the large amounts of organic matter that receive these areas, which produce principally an intensification of the organic carbon remineralization and a decrease of the oxygen and pH levels (Wallace et al., 2014; Carstensen and Duarte, 2019; Capelle et al., 2020). Different studies focused on understanding long-term drivers of pH, have revealed that the pH decline in coastal environments can be larger than the one predicted from ocean acidification (Cai et al., 2011; Duarte et al., 2013; Carstensen and Duarte, 2019; Shen et al., 2020). Cai et al. (2011) suggest that eutrophication could increase the susceptibility of coastal waters to ocean acidification. Borges and Gypens (2010) also found that the response of carbonate chemistry to changes of nutrient inputs to the coastal zone is stronger than ocean acidification. In Guanabara Bay (Brazil), Cotovicz et al. (2018) found that, changes in the aquatic carbonate chemistry seemed to be more affected by the biological metabolism than by changes related to the increase of atmospheric CO_2 concentrations. Xue et al. (2017) also suggested that interannual ΩAr changes due to riverine inputs could be greater than the changes due to a continue rise of atmospheric CO_2 over the past few decades in the Gray's Reef National Marine Sanctuary (Georgia, United States).

In deep ocean, the declining rates of pH and ΩAr are lower. Bates and Peters (2007) and Doney et al. (2009) obtained a pH decrease of −0.0017 yr^{-1} (1983–2005) and −0.0019 yr^{-1} (1988–2007) in the subtropical North Atlantic Ocean and in the North Pacific Ocean, respectively. These authors also determined a decrease rate for ΩAr of −0.006 ± 0.001 yr^{-1} and −0.0069 yr^{-1} for the same areas. This difference between coastal and open waters reflects the greater vulnerability of the coastal areas to the combined stresses of complex hydrodynamics, biological processes and effect of eutrophication (e.g. Thomas et al., 2007; Cai et al., 2011; Duarte et al., 2013).

5. Conclusions

The results obtained in this study reveal that the GoC is oversaturated of $CaCO_3$ in the whole water column, and the highest values of ΩAr were found in the SML. TA, pH_T and ΩAr show a high spatial variability in the SML related to the complex hydrodynamics of this transition zone between the coastal area and the continental shelf of the GoC. The presence of the warmer eastward branch of the Azores Current in the distal waters and the drift of the filament off from Cape St. Vincent upwelling in the northwest zone produce a significant increase in TA, pH_T and ΩAr. An increase in ΩAr can also be appreciated in the coastal area near the Guadalquivir estuary, which constitutes the main continental input of TA and Ca^{2+} in GoC. Additionally, the existence of

other upwelling processes, along the African coast and in the Trafalgar coast, contributes to the variability of ΩAr found in the SML. Superimposed to spatial trends, vertical variations of ΩAr have been found in the SML. The highest values are observed in the surface zone (~5 m), where the interaction with the atmosphere contributes to keep relatively high pH_T values. A decrease in pH and ΩAr with depth through the maximum Chl and maximum AOU layers has also been detected.

ΩAr changes have been decomposed in factors to establish the main processes that control its variability in the SML. The in situ biological activity is the primary process that affects the ΩAr changes (±0.6), while temperature variation (±0.05), mixing processes (±0.05) and the exchange of CO_2 with the atmosphere (±0.02) have a lower relative importance. In the other hand, the buffer capacity also appears to be controlled by changes in biological activity, as shown from the relationships found with TA/DIC and AOU. A variation of the buffer factors with temperature has also been found, which is related to its effect on the equilibrium of the inorganic carbonate system.

In addition, the TA and $[Ca^{2+}]$ in deeper waters ($z > 100$ m) showed a conservative behaviour with S_P, recording the highest values (2465 ± 9 μmol kg^{-1} and 11.32 ± 0.12 mmol kg^{-1}, respectively) in those depths where MOW water mass was located. AOU values were also higher in MOW, related to the organic matter mineralization that occurs in the Mediterranean basin. In contrast, pH and ΩAr decreased with depth due to the organic matter mineralization processes.

In turn, the GoC's waters situated closer to the coast, showed a significative acidification from 2006 to 2016, with decrease slopes of -0.0089 yr^{-1} for pH and -0.0552 yr^{-1} for ΩAr. However, this average reduction was more intense than the expected due to the increase of the atmospheric CO_2 levels over this period of time, since this area is largely overshadowed by local and regional variability from biological activity, continental inputs, changes in hydrography and mixed layer dynamics. Despite the fact that this study offers the first results of the $CaCO_3$ saturation state trend in the coastal areas of the GoC, more studies are necessary to be able to establish the possible acidification in offshore and deeper waters in the GoC.

CRediT authorship contribution statement

Dolores Jiménez-López: Investigation, Writing – original draft, Writing – review & editing. **Teodora Ortega:** Supervision, Investigation, Writing – review & editing. **Ana Sierra:** Investigation, Writing – review & editing. **Rocío Ponce:** Investigation. **Abelardo Gómez-Parra:** Investigation. **Jesús Forja:** Supervision, Investigation, Writing – review & editing.

Declaration of competing interest

The authors declare that they have no known competing financial interests or personal relationships that could have appeared to influence the work reported in this paper.

Acknowledgements

The authors would like to thank the crews of the R/V's Angeles Alvariño and Ramón Margalef for their assistance during fieldwork. We also thank the three anonymous reviewers and to the editor for their comments provided, which helped substantially to improve this article.

Funding

This work was funded by the Spanish CICYT (Spanish Program for Science and Technology) under the contract RTI2018-100865-B-C21. Dolores Jiménez-López was financed by the University of Cádiz with a FPI fellowship (FPI-UCA) and Ana Sierra was financed by the Spanish Ministry of Education with a FPU fellowship (FPU2014-04048).

Appendix A. Supplementary data

Supplementary data to this article can be found online at https://doi.org/10.1016/j.scitotenv.2021.147858.

References

Aberle, N., Schulz, K.G., Stuhr, A., Malzahn, A.M., Ludwig, A., Riebesell, U., 2013. High tolerance of microzooplankton to ocean acidification in an Arctic coastal plankton community. Biogeosciences 10, 1471–1481. https://doi.org/10.5194/bg-10-1471-2013.

Aït-Ameur, N., Goyet, C., 2006. Distribution and transport of natural and anthropogenic CO_2 in the Gulf of Cádiz. Deep-Sea Res. II Top. Stud. Oceanogr. 53, 1329–1343. https://doi.org/10.1016/j.dsr2.2006.04.003.

Álvarez, M., Sanleón-Bartolomé, H., Tanhua, T., Mintrop, L., Luchetta, A., Cantoni, C., Civitarese, G., 2014. The CO_2 system in the Mediterranean Sea: a basin wide perpective. Ocean Sci. 10, 69–92. https://doi.org/10.5194/os-10-69-2014.

Amaral, V., Romera-Castillo, C., Forja, J., 2020. Dissolved organic matter in the Gulf of Cádiz: distribution and drivers of chromophoric and fluorescent properties. Front. Mar. Sci. 7, 1–15. https://doi.org/10.3389/fmars.2020.00126.

Andersson, A.J., MacKenzie, F.T., 2012. Revisiting four scientific debates in ocean acidification research. Biogeosciences 9, 893–905. https://doi.org/10.5194/bg-9-893-2012.

Baringer, M.O.N., Price, J.F., 1999. A review of the physical oceanography of the Mediterranean outflow. Mar. Geol. 155, 63–82. https://doi.org/10.1016/S0025-3227(98)00141-8.

Bates, N.R., Peters, A.J., 2007. The contribution of atmospheric acid deposition to ocean acidification in the subtropical North Atlantic Ocean. Mar. Chem. 107, 547–558. https://doi.org/10.1016/j.marchem.2007.08.002.

Bellanco, M.J., Sánchez-Leal, R.F., 2016. Spatial distribution and intra-annual variability of water masses on the Eastern Gulf of Cádiz seabed. Cont. Shelf Res. 128, 26–35. https://doi.org/10.1016/j.csr.2016.09.001.

Benson, B.B., Krause Jr., D., 1984. The concentration and isotopic fractionation of oxygen dissolved in freshwater and seawater in equilibrium with the atmosphere. Limnol. Oceanogr. 29, 620–632. https://doi.org/10.4319/lo.1984.29.3.0620.

Bindoff, N.L., Cheung, W.W.L., Kairo, J.G., 2019. Changing ocean, marine ecosystems, and dependent communities. IPCC Special Report on the Ocean and Cryosphere in a Changing Climate. Intergovernmental Panel on Climate Change, Switzerland, pp. 477–587.

Borges, A.V., Gypens, N., 2010. Carbonate chemistry in the coastal zone responds more strongly to eutrophication than ocean acidification. Limnol. Oceanogr. 55, 346–353. https://doi.org/10.4319/lo.2010.55.1.0346.

Cai, W.-J., Hu, X., Huang, W.J., Murrell, M.C., Lehrter, J.C., Lohrenz, S.E., Chou, W.C., Zhai, W., Hollibaugh, J.T., Wang, Y., Zhao, P., Guo, X., Gundersen, K., Dai, M., Gong, G.C., 2011. Acidification of subsurface coastal waters enhanced by eutrophication. Nat. Geosci. 4, 766–770. https://doi.org/10.1038/ngeo1297.

Cai, W.-J., Huang, W.-J., Luther III, G.W., Pierrot, D., Testa, J., Li, M., Xue, M., Joesoef, A., Mann, R., Brodeur, J., Xu, Y., Chen, B., Hussain, N., Waldbusser, G.G., Cornwell, J., Kemp, W.M., 2017. Redox reactions and weak buffering capacity lead to acidification in the Chesapeake Bay. Nat. Commun. 8, 369. https://doi.org/10.1038/s41467-017-00417-7.

Caldeira, K., Wickett, M., 2005. Ocean model predictions of chemistry changes from carbon dioxide emissions to the atmosphere and ocean. J. Geophys. Res. Oceans 110, 1–12. https://doi.org/10.1029/2004JC002671.

Capelle, D.W., Kuzyk, Z.Z.A., Papakyriakou, T., Guéguen, C., Miller, L.A., Macdonald, R.W., 2020. Effect of terrestrial organic matter on ocean acidification and CO_2 flux in an Arctic shelf sea. Prog. Oceanogr. 185, 102319. https://doi.org/10.1016/j.pocean.2020.102319.

Carracedo, L.I., Pardo, P.C., Flecha, S., Pérez, F.F., 2016. On the Mediterranean water composition. J. Phys. Oceanogr. 46, 1339–1358. https://doi.org/10.1175/JPO-D-15-0095.1.

Carstensen, J., Duarte, C.M., 2019. Drivers of pH variability in coastal ecosystems. Environ. Sci. Technol. 53, 4020–4029. https://doi.org/10.1021/acs.est.8b03655.

Confederación Hidrográfica del Guadalquivir, España, d. Sistema Automático de Información Hidrológica. Datos Históricoshttp://www.chguadalquivir.es/saih/DatosHistoricos.aspx (accessed 25 September 2020).

Cotovicz, L.C., Knoppers, B.A., Brandini, N., Poirier, D., Costa Santos, S.J., Abril, G., 2018. Aragonite saturation state in a tropical coastal embayment dominated by phytoplankton blooms (Guanabara Bay - Brazil). Mar. Pollut. Bull. 129, 729–739. https://doi.org/10.1016/j.marpolbul.2017.10.064.

Criado-Aldeanueva, F., García-Lafuente, J., Vargas, J.M., Del Río, J., Vázquez, A., Reul, A., Sánchez, A., 2006. Distribution and circulation of water masses in the Gulf of Cádiz from in situ observations. Deep-Sea Res. II Top. Stud. Oceanogr. 53, 1144–1160. https://doi.org/10.1016/j.dsr2.2006.04.012.

Criado-Aldeanueva, F., García-Lafuente, J., Navarro, G., Ruiz, J., 2009. Seasonal and interannual variability of the surface circulation in the eastern Gulf of Cadiz (SW Iberia). J. Geophys. Res. Oceans 114, 1–11. https://doi.org/10.1029/2008JC005069.

Culkin, F., Cox, R.A., 1966. Sodium, potassium, magnesium, calcium and strontium in sea water. Deep-Sea Res. Oceanogr. Abstr. 13, 789–804. https://doi.org/10.1016/0011-7471(76)90905-0.

Dafner, E.V., González-Dávila, M., Santana-Casiano, J.M., Sempere, R., 2001. Total organic and inorganic carbon exchange through the Strait of Gibraltar in September 1997. Deep-Sea Res. I Oceanogr. Res. Pap. 48, 1217–1235. https://doi.org/10.1016/S0967-0637(00)00064-9.

de Carvalho-Borges, M., Orselli, I.B.M., Ferreira, M.L. de C., Kerr, R., 2018. Seawater acidification and anthropogenic carbon distribution on the continental shelf and slope of

the western South Atlantic Ocean. J. Mar. Syst. 187, 62–81. https://doi.org/10.1016/j.jmarsys.2018.06.008.
de la Paz, M., Gómez-Parra, A., Forja, J., 2007. Inorganic carbon dynamic and air-water CO_2 exchange in the Guadalquivir Estuary (SW Iberian Península). J. Mar. Syst. 68, 265–277. https://doi.org/10.1016/j.jmarsys.2006.11.011.
de la Paz, M., Debelius, B., Macías, D., Vázquez, A., Gómez-Parra, A., Forja, J.M., 2008. Tidal-induced inorganic carbon dynamics in the Strait of Gibraltar. Cont. Shelf Res. 28, 1827–1837. https://doi.org/10.1016/j.csr.2008.04.012.
de la Paz, M., Huertas, E.M., Padín, X.A., Gónzalez-Dávila, M., Santana-Casiano, M., Forja, J.M., Orbi, A., Pérez, F.F., Ríos, A.F., 2011. Reconstruction of the seasonal cycle of air-sea CO_2 fluxes in the Strait of Gibraltar. Mar. Chem. 126, 155–162. https://doi.org/10.1016/j.marchem.2011.05.004.
Dickson, A.G., 1990. Thermodynamics of the dissociation of boric acid in synthetic seawater from 273.15 to 318.15 K. Deep-Sea Res. A Oceanogr. Res. Pap. 37, 755–766. https://doi.org/10.1016/0198-0149(90)90004-F.
Dickson, A.G., Millero, F.J., 1987. A comparison of the equilibrium constants for the dissociation of carbonic acid in seawater media. Deep-Sea Res. A Oceanogr. Res. Pap. 34, 1733–1743. https://doi.org/10.1016/0198-0149(87)90021-5.
Dickson, A.G., Sabine, C.L., Christian, J.R., 2007. Guide to Best Practices for Ocean CO_2 Measurements. Sidney, British Columbia, North Pacific Marine Science Organization (191 pp.).
Díez-Minguito, M., Contreras, E., Polo, M.J., Losada, M.A., 2013. Spatio-temporal distribution, along-channel transport, and post-riverflood recovery of salinity in the Guadalquivir estuary (SW Spain). J. Geophys. Res. Oceans 118, 2267–2278. https://doi.org/10.1002/jgrc.20172.
Dinauer, A., Mucci, A., 2018. Distinguishing between physical and biological controls on the spatial variability of pCO_2: a novel approach using OMP water mass analysis (St. Lawrence, Canada). Mar. Chem. 204, 107–120. https://doi.org/10.1016/j.marchem.2018.03.007.
Doney, S.C., 2006. The dangers of ocean acidification. Sci. Am. 294, 58–65. https://doi.org/10.1038/scientificamerican0306-58.
Doney, S.C., Fabry, V.J., Feely, R.A., Kleypas, J.A., 2009. Ocean acidification: the other CO_2 problem. Annu. Rev. Mar. Sci. 1, 169–192. https://doi.org/10.1146/annurev.marine.010908.163834.
Duarte, C.M., Hendriks, I.E., Moore, T.S., Olsen, Y.S., Steckbauer, A., Ramajo, L., Carstensen, J., Trotter, J.A., McCulloch, M., 2013. Is ocean acidification an open-ocean syndrome? Understanding anthropogenic impacts on seawater pH. Estuar. Coasts 36, 221–236. https://doi.org/10.1007/s12237-013-9594-3.
Dupont, S., Dorey, N., Thorndyke, M., 2010. What meta-analysis can tell us about vulnerability of marine biodiversity to ocean acidification? Estuar. Coast. Shelf Sci. 89, 182–185. https://doi.org/10.1016/j.ecss.2010.06.013.
Egleston, E.S., Sabine, C.L., Morel, F.M.M., 2010. Revelle revisited: buffer factors that quantify the response of ocean chemistry to changes in DIC and alkalinity. Glob. Biogeochem. Cycles 24, GB1002. https://doi.org/10.1029/2008GB003407.
Eyre, B.D., Cyronak, T., Drupp, P., De Carlo, E.H., Sachs, J.P., Andersson, A.J., 2018. Coral reefs will transition to net dissolving before end of century. Science 359, 908–911. https://doi.org/10.1126/science.aao1118.
Feely, R.A., Doney, S.C., Cooley, S.R., 2009. Ocean acidification: present conditions and future changes in a high-CO_2 world. Oceanography 22, 36e47. https://doi.org/10.5670/oceanog.2009.95.
Feely, R.A., Alin, S.R., Newton, J., Sabine, C.L., Warner, M., Devol, A., Krembs, C., Maloy, C., 2010. The combined effects of ocean acidification, mixing, and respiration on pH and carbonate saturation in an urbanized estuary. Estuar. Coast. Shelf Sci. 88, 442–449. https://doi.org/10.1016/j.ecss.2010.05.004.
Ferrón, S., Alonso-Pérez, F., Anfuso, E., Murillo, F.J., Ortega, T., Castro, C.G., Forja, J.M., 2009. Benthic nutrient recycling on the northeastern shelf of the Gulf of Cádiz (SW Iberian Peninsula). Mar. Ecol. Prog. Ser. 390, 79–95. https://doi.org/10.3354/meps08199.
Flecha, S., Pérez, F.F., Navarro, G., Ruiz, J., Olivé, I., Rodríguez-Gálvez, S., Costas, E., Huertas, I.E., 2012. Anthropogenic carbon inventory in the Gulf of Cádiz. J. Mar. Syst. 92, 67–75. https://doi.org/10.1016/j.jmarsys.2011.10.010.
Flecha, S., Pérez, F.F., Murata, A., Makaoui, A., Huertas, I.E., 2019. Decadal acidification in Atlantic and Mediterranean water masses exchanging at the Strait of Gibraltar. Sci. Rep. 9, 1–11. https://doi.org/10.1038/s41598-019-52084-x.
Freitas, P.S., Abrantes, F., 2002. Suspended particulate matter in the Mediterranean water at the Gulf of Cadiz and off the southwest coast of the Iberian Peninsula. Deep-Sea Res. II Top. Stud. Oceanogr. 49, 4245–4261. https://doi.org/10.1016/S0967-0645(02)00153-4.
Gattuso, J.P., Magnan, A., Billé, R., Cheung, W.W.L., Howes, E.L., Joos, F., Allemand, D., Bopp, L., Cooley, S.R., Eakin, C.M., Hoegh-Guldberg, O., Kelly, R.P., Pörtner, H.O., Rogers, A.D., Baxter, J.M., Laffoley, D., Osborn, D., Rankovic, A., Rochette, J., Sumaila, U.R., Treyer, S., Turley, C., 2015. Contrasting futures for ocean and society from different anthropogenic CO_2 emissions scenarios. Science 349, aac4722. https://doi.org/10.1126/science.aac4722.
González-Dávila, M., Santana-Casiano, J.M., Dafner, E.V., 2003. Winter mesoscale variations of carbonate system parameters and estimates of CO_2 fluxes in the Gulf of Cádiz, northeast Atlantic Ocean (February 1998). J. Geophys. Res. 108, 1–11. https://doi.org/10.1029/2001JC001243.
González-García, C., Forja, J., González-Cabrera, M.C., Jiménez, M.P., Lubián, L.M., 2018. Annual variations of total and fractionated chlorophyll and phytoplankton groups in the Gulf of Cádiz. Sci. Total Environ. 613, 1551–1565. https://doi.org/10.1016/j.scitotenv.2017.08.292.
González-Ortegón, E., Drake, P., 2012. Effects of freshwater inputs on the lower trophic levels of a temperate estuary: physical, physiological or trophic forcing? Aquat. Sci. 74, 455–469. https://doi.org/10.1007/s00027-011-0240-5.
Gould, W.J., 1985. Physical oceanography of the Azores Front. Prog. Oceanogr. 14, 167–190. https://doi.org/10.1016/0079-6611(85)90010-2.
Granado-Lorencio, C., 1991. The effect of man on the fish fauna of the river Guadalquivir, Spain. Fish. Res. 12, 91–100. https://doi.org/10.1016/0165-7836(91)90034-D.
Grasshoff, K., Erhardt, M., Kremiling, K., 1983. Methods of Seawater Analysis. Verlag Chemie, New York (419 pp.).
Hauck, J., Zeising, M., Le Quéré, C., Gruber, N., Bakker, D.C.E., Bopp, L., Chau, T.T.T., Gürses, Ö., Ilyina, T., Landschützer, P., Lenton, A., Resplandy, L., Rödenbeck, C., Schwinger, J., Séférian, R., 2020. Consistency and challenges in the ocean carbon sink estimate for the global carbon budget. Front. Mar. Sci. 7, 1–22. https://doi.org/10.3389/fmars.2020.571720.
Hernández-Molina, F.J., Stow, D.A.V., Alvarez-Zarikian, C.A., Acton, G., Bahr, A., Balestra, B., Ducassou, E., Flood, R., Flores, J.-A., Furota, S., Grunert, P., Hodell, D., Jimenez-Espejo, F., Kim, J.K., Krissek, L., Kuroda, J., Li, B., Llave, E., Lofi, J., Lourens, L., Miller, M., Nanayama, F., Nishida, N., Richter, C., Roque, C., Pereira, H., Goni, M.F.S., Sierro, F.J., Singh, A.D., Sloss, C., Takashimizu, Y., Tzanova, A., Voelker, A., Williams, T., Xuan, C., 2014. Onset of Mediterranean outflow into the North Atlantic. Science 344, 1244–1250. https://doi.org/10.1126/science.1251306.
Hofmann, E.E., Cahill, B., Fennel, K., Friedrichs, M.A.M., Hyde, K., Lee, C., Mannino, A., Najjar, R.G., O'Reilly, J.E., Wilkin, J., Xue, J., 2011. Modeling the dynamics of continental shelf carbon. Annu. Rev. Mar. Sci. 3, 93–122. https://doi.org/10.1146/annurev-marine-120709-142740.
Hu, X., Li, Q., Huang, W.J., Chen, B., Cai, W.J., Rabalais, N.N., Eugene Turner, R., 2017. Effects of eutrophication and benthic respiration on water column carbonate chemistry in a traditional hypoxic zone in the Northern Gulf of Mexico. Mar. Chem. 194, 33–42. https://doi.org/10.1016/j.marchem.2017.04.004.
Hu, X., Nuttall, M.F., Wang, H., Yao, H., Staryk, C.J., McCutcheon, M.R., Eckert, R.J., Embesi, J.A., Johnston, M.A., Hickerson, E.L., Schmahl, G.P., Manzello, D., Enochs, I.C., DiMarco, S., Barbero, L., 2018. Seasonal variability of carbonate chemistry and decadal changes in waters of a marine sanctuary in the Northwestern Gulf of Mexico. Mar. Chem. 205, 16–28. https://doi.org/10.1016/j.marchem.2018.07.006.
Huertas, E., Navarro, G., Rodríguez-Gálvez, S., Prieto, L., 2005. The influence of phytoplankton biomass on the spatial distribution of carbon dioxide in surface sea water of a coastal area of the Gulf of Cádiz (southwestern Spain). Can. J. Bot. 83, 929–940. https://doi.org/10.1139/b05-082 2005.
Huertas, I.E., Navarro, G., Rodríguez-Gálvez, S., Lubián, L.M., 2006. Temporal patterns of carbon dioxide in relation to hydrological conditions and primary production in the northeastern shelf of the Gulf of Cádiz (SW Spain). Deep-Sea Res. II Top. Stud. Oceanogr. 53, 1344–1362. https://doi.org/10.1016/j.dsr2.2006.03.010.
Huertas, I.E., Ríos, A.F., García-Lafuente, J., Makaoui, A., Rodríguez-Gálvez, S., Sánchez-Román, A., Orbi, A., Ruíz, J., Pérez, F.F., 2009. Anthropogenic and natural CO_2 exchange through the Strait of Gibraltar. Biogeosciences 6, 647–662. https://doi.org/10.5194/bg-6-647-2009.
Jiang, L.Q., Feely, R.A., Carter, B.R., Greeley, D.J., Gledhill, D.K., Arzayus, K.M., 2015. Climatological distribution of aragonite saturation state in the global oceans. Glob. Biogeochem. Cycles 29, 1656–1673. https://doi.org/10.1002/2015GB005198.
Jiang, L.Q., Carter, B.R., Feely, R.A., Lauvset, S.K., Olsen, A., 2019. Surface ocean pH and buffer capacity: past, present and future. Sci. Rep. 9, 18624. https://doi.org/10.1038/s41598-019-55039-4.
Jiménez-López, D., Sierra, A., Ortega, T., Garrido, S., Hernández-Puyuelo, N., Sánchez-Leal, R., Forja, J., 2019. pCO_2 variability in the surface waters of the eastern Gulf of Cádiz (SW Iberian Peninsula). Ocean Sci. 15, 1225–1245. https://doi.org/10.5194/os-15-1225-2019.
Johnson, J., Stevens, I., 2000. A fine resolution model of the eastern North Atlantic between the Azores, the Canary Islands and the Gibraltar Strait. Deep-Sea Res. I Oceanogr. Res. Pap. 47, 875–899. https://doi.org/10.1016/S0967-0637(99)00073-4 2000.
Johnson, Z.I., Wheeler, B.J., Blinebry, S.K., Carlson, C.M., Ward, C.S., Hunt, D.E., 2013. Dramatic variability of the carbonate system at a temperate coastal ocean site (Beaufort, North Carolina, USA) is regulated by physical and biogeochemical processes on multiple timescales. PLoS One 8, 1–8. https://doi.org/10.1371/journal.pone.0085117.
Joos, F., Spahni, R., 2008. Rates of change in natural and anthropogenic radiative forcing over the past 20,000 years. Proc. Natl. Acad. Sci. U. S. A. 105, 1425–1430. https://doi.org/10.1073/pnas.0707386105.
Karstensen, J., Tomczak, M., 1998. Age determination of mixed water masses using CFC and oxygen data. J. Geophys. Res. Oceans 103, 18599–18609. https://doi.org/10.1029/98JC00889.
Käse, R.H., Zenk, W., Sanford, T.B., Hiller, W., 1985. Currents, fronts and eddy fluxes in the Canary Basin. Prog. Oceanogr. 14, 231–257. https://doi.org/10.1016/0079-6611(85)90013-8.
Landschützer, P., Ilyina, T., Lovenduski, N.S., 2019. Detecting regional modes of variability in observation-based surface ocean pCO_2. Geophys. Res. Lett. 46, 2670–2679. https://doi.org/10.1029/2018GL081756.
Lee, K., Kim, T.W., Byrne, R.H., Millero, F.J., Feely, R.A., Liu, Y.M., 2010. The universal ratio of boron to chlorinity for the North Pacific and North Atlantic oceans. Geochim. Cosmochim. Acta 74, 1801–1811. https://doi.org/10.1016/j.gca.2009.12.027.
Leung, J.Y.S., Doubleday, Z.A., Nagelkerken, I., Chen, Y.J., Xie, Z.H., Connell, S.D., 2019. How calorie-rich food could help marine calcifiers in a CO_2-rich future. Proc. R. Soc. B Biol. Sci. 286, 20190757. https://doi.org/10.1098/rspb.2019.0757.
Li, C.L., Zhai, W.D., 2019. Decomposing monthly declines in subsurface-water pH and aragonite saturation state from spring to autumn in the North Yellow Sea. Cont. Shelf Res. 185, 37–50. https://doi.org/10.1016/j.csr.2018.11.003.
Li, X., Bellerby, R.G.J., Wallhead, P., Ge, J., Liu, J., Liu, J., Yang, A., 2020. A neural network-based analysis of the seasonal variability of surface total alkalinity on the East China Sea shelf. Front. Mar. Sci. 7, 1–13. https://doi.org/10.3389/fmars.2020.00219.
Millero, F.J., 1979. The thermodynamics of the carbonate system in seawater. Geochim. Cosmochim. Acta 43, 1651–1661. https://doi.org/10.1016/0016-7037(79)90184-4.

Millero, F.J., 2007. The marine inorganic carbon cycle. Chem. Rev. 107, 308–341. https://doi.org/10.1021/cr0503557.
Millero, F.J., 2010. Carbonate constants for estuarine waters. Mar. Freshw. Res. 61, 139–142. https://doi.org/10.1071/MF09254.
Millero, F.J., Poisson, A., 1981. International one-atmosphere equation of state of seawater. Deep-Sea Res. A Oceanogr. Res. Pap. 28, 625–629. https://doi.org/10.1016/0198-0149(81)90122-9.
Morse, J.W., Andersson, A.J., Mackenzie, F.T., 2006. Initial responses of carbonate-rich shelf sediments to rising atmospheric pCO_2 and "ocean acidification": role of high Mg-calcites. Geochim. Cosmochim. Acta 70, 5814–5830. https://doi.org/10.1016/j.gca.2006.08.017.
Morse, J.W., Arvidson, R.S., Lüttge, A., 2007. Calcium carbonate formation and dissolution. Chem. Rev. 107, 342–381. https://doi.org/10.1021/cr050358j.
Mucci, A., 1983. The solubility of calcite and aragonite in seawater at various salinities, temperatures, and one atmosphere total pressure. Am. J. Sci. 283, 781–799. https://doi.org/10.2475/ajs.283.7.780.
Olsen, A., Lange, N., Key, R.M., Tanhua, T., Álvarez, M., Becker, S., Bittig, H.C., Carter, B.R., Cotrim da Cunha, L., Feely, R.A., van Heuven, S., Hoppema, M., Ishii, M., Jeansson, E., Jones, S.D., Jutterström, S., Karlsen, M.K., Kozyr, A., Lauvset, S.K., Lo Monaco, C., Murata, A., Pérez, F.F., Pfeil, B., Schirnick, C., Steinfeldt, R., Suzuki, T., Telszewski, M., Tilbrook, B., Velo, A., Wanninkhof, R., 2019. GLODAPv2.2019 - an update of GLODAPv2. Earth Syst. Sci. Data 11, 1437–1461. https://doi.org/10.5194/essd-11-1437-2019.
Orr, J.C., Fabry, V.J., Aumont, O., Bopp, L., Doney, S.C., Feely, R.A., Gnanadesikan, A., Gruber, N., Ishida, A., Joos, F., Key, R.M., Lindsay, K., Maier-Reimer, E., Matear, R., Monfray, P., Mouchet, A., Najjar, R.G., Plattner, G.K., Rodgers, K.B., Sabine, C.L., Sarmiento, J.L., Schlitzer, R., Slater, R.D., Totterdell, I.J., Weirig, M.F., Yamanaka, Y., Yool, A., 2005. Anthropogenic ocean acidification over the twenty-first century and its impact on calcifying organisms. Nature 437, 681–686. https://doi.org/10.1038/nature04095.
Parrilla, G., 1998. Mid-Term Scientific Report, CANIGO-MAST 3-CT 96-0060. Institute of Esp. Oceanography, Madrid (321 pp.).
Parsons, T.R., Maita, Y., Lalli, C.M., 1984. A Manual of Chemical and Biological Methods for Seawater Analysis. Pergamon Press, Oxford (172 pp.).
Peliz, A., Marchesiello, P., Santos, A.M.P., Dubert, J., Teles-Machado, A., Marta-Almeida, M., Le Cann, B., 2009. Surface circulation in the Gulf of Cádiz: 2. Inflow-outflow coupling and the Gulf of Cádiz slope current. J. Geophys. Res. Oceans 114, 1–16. https://doi.org/10.1029/2008JC004771.
Pérez, F.F., Castro, C.G., Álvarez-Salgado, X.A., Ríos, A.F., 2001. Coupling between the Iberian basin - scale circulation and the Portugal boundary current system: a chemical study. Deep-Sea Res. I Oceanogr. Res. Pap. 48, 1519–1533. https://doi.org/10.1016/S0967-0637(00)00101-1.
Pérez, F.F., Álvarez, M., Ríos, A.F., 2002. Improvements on the back calculation technique for estimating anthropogenic CO_2. Deep-Sea Res. I Oceanogr. Res. Pap. 49, 859–875. https://doi.org/10.1016/S0967-0637(02)00002-X.
Pierrot, D., Lewis, E., Wallace, D.W.R., 2006. MS Excel Program Developed for CO_2 System Calculations. https://doi.org/10.3334/CDIAC/otg.CO2SYS_XLS_CDIAC105a.
Poole, R., Tomczak, M., 1999. Optimum multiparameter analysis of the water mass structure in the western North Atlantic Ocean. J. Geophys. Res. 98, 10155. https://doi.org/10.1029/93jc00180.
Prieto, L., Garcia, C.M., Corzo, A., Ruiz Segura, J., Echevarria, F., 1999. Phytoplankton, bacterioplankton and nitrate reductase activity distribution in relation to physical structure in the northern Alboran Sea and Gulf of Cádiz (southern Iberian Península). Bol. Inst. Esp. Oceanogr. 15, 401–411.
Ramajo, L., Pérez-León, E., Hendriks, I.E., Marbà, N., Krause-Jensen, D., Sejr, M.K., Blicher, M.E., Lagos, N.A., Olsen, Y.S., Duarte, C.M., 2016. Food supply confers calcifiers resistance to ocean acidification. Sci. Rep. 6, 19374. https://doi.org/10.1038/srep19374.
Relvas, P., Barton, E.D., 2002. Mesoscale patterns in the Cape São Vicente (Iberian Peninsula) upwelling region. J. Geophys. Res. Oceans 107, 1–23. https://doi.org/10.1029/2000jc000456.
Rhein, M., Hinrichsen, H.H., 1993. Modification of Mediterranean water in the Gulf of Cadiz, studied with hydrographic, nutrient and chlorofluoromethane data. Deep-Sea Res. I Oceanogr. Res. Pap. 40, 267–291. https://doi.org/10.1016/0967-0637(93)90004-M.
Ribas-Ribas, M., Gómez-Parra, A., Forja, J.M., 2011. Seasonal distribution of the inorganic carbon system and net ecosystem production in the north eastern shelf of the Gulf of Cádiz (Southwest Iberian Peninsula). Cont. Shelf Res. 31, 1931–1942. https://doi.org/10.1016/j.csr.2011.09.003.
Ries, J.B., Cohen, A.L., McCorkle, D.C., 2009. Marine calcifiers exhibit mixed responses to CO_2-induced ocean acidification. Geology 37, 1131–1134. https://doi.org/10.1130/G30210A.1.
Ríos, A.F., Resplandy, L., García-Ibáñez, M.I., Fajar, N.M., Velo, A., Padin, X.A., Wanninkhof, R., Steinfeldt, R., Rosón, G., Pérez, F.F., 2015. Decadal acidification in the water masses of the Atlantic Ocean. Proc. Natl. Acad. Sci. U. S. A. 112, 9950–9955. https://doi.org/10.1073/pnas.1504613112.
Rosón, G., Guallart, E.F., Pérez, F.F., Ríos, A.F., 2016. Calcium distribution in the subtropical Atlantic Ocean: implications for calcium excess and saturation horizons. J. Mar. Syst. 158, 45–51. https://doi.org/10.1016/j.jmarsys.2016.01.011.
Ruiz, J., Polo, M.J., Díez-Minguito, M., Navarro, G., Morris, E.P., Huertas, E., Caballero, I., Contreras, E., Losada, M.A., 2015. The Guadalquivir estuary: a hot spot for environmental and human conflicts. In: Finkl, C.W., Makowski, C. (Eds.), Environmental Management and Governance. Springer, International Publishing Switzerland, pp. 199–232.
Sabine, C.L., Feely, R.A., 2007. The oceanic sink for carbon dioxide. In: Reay, D., Hewitt, C.N., Smith, K., Grace, J. (Eds.), Greenhouse Gas Sinks. CABI Publishing, Oxfordshire, UK, pp. 31–49.
Sánchez-Leal, R.F., Bellanco, M.J., Fernández-Salas, L.M., García-Lafuente, J., Gasser-Rubinat, M., González-Pola, C., Hernández-Molina, F.J., Pelegrí, J.L., Peliz, A., Relvas, P., Roque, D., Ruiz-Villarreal, M., Sammartino, S., Sánchez-Garrido, J.C., 2017. The Mediterranean overflow in the Gulf of Cádiz: a rugged journey. Sci. Adv. 3, eaao0609. https://doi.org/10.1126/sciadv.aao0609.
Santana-Casiano, J.M., Gonzalez-Davila, M., Laglera, L.M., 2002. The carbon dioxide system in the Strait of Gibraltar. Deep-Sea Res. II Top. Stud. Oceanogr. 49, 4145–4161. https://doi.org/10.1016/S0967-0645(02)00147-9.
Shen, C., Testa, J.M., Li, M., Cai, W.-J., 2020. Understanding anthropogenic impacts on pH and aragonite saturation state in Chesapeake Bay: insights from a 30-year model study. J. Geophys. Res. Biogeosci. 125, e2019JG005620. https://doi.org/10.1029/2019JG005620.
Siegenthaler, U., Stocker, T.F., Monnin, E., Lüthi, D., Schwander, J., Stauffer, B., Raynaud, D., Barnola, J.-M., Fischer, H., Masson-Delmotte, V., Jouzel, J., 2005. Stable carbon cycle–climate relationship during the Late Pleistocene. Science 310, 1313–1317. https://doi.org/10.1126/science.1120130.
Sierra, A., Jiménez-López, D., Ortega, T., Ponce, R., Bellanco, M.J., Sánchez-Leal, R., Gómez-Parra, A., Forja, J., 2017. Distribution of N_2O in the eastern shelf of the Gulf of Cadiz (SW Iberian Peninsula). Sci. Total Environ. 593–594, 796–808. https://doi.org/10.1016/j.scitotenv.2017.03.189.
Stanichny, S., Tigny, V., Stanichnaya, R., Djenidi, S., 2005. Wind driven upwelling along the African coast of the Strait of Gibraltar. Geophys. Res. Lett. 32, 1–4. https://doi.org/10.1029/2004GL021760.
Thomas, H., Prowe, A.E.F., van Heuven, S., Bozec, Y., de Baar, H.J.W., Schiettecatte, L.S., Suykens, K., Koné, M., Borges, A.V., Lima, I.D., Doney, S.C., 2007. Rapid decline of the CO_2 buffering capacity in the North Sea and implications for the North Atlantic Ocean. Glob. Biogeochem. Cycles 21, 1–13. https://doi.org/10.1029/2006GB002825.
Thompson, R.O.R., 1976. Climatological numerical models of the surface mixed layer of the ocean. J. Phys. Oceanogr. 6, 496–503. https://doi.org/10.1175/1520-0485(1976)006<0496:CNMOTS>2.0.CO;2.
Tomczak Jr., M., 1981. A multi-parameter extension of temperature/salinity diagram techniques for the analysis of non-isopycnal mixing. Prog. Oceanogr. 10, 147–171. https://doi.org/10.1016/0079-6611(81)90010-0.
Tomczak, M., Large, D.G.B., 1989. Optimum multiparameter analysis of mixing in the thermocline of Indian Ocean. J. Geophys. Res. Oceans 94, 16141–16149. https://doi.org/10.1029/JC094iC11p16141.
Tynan, E., Tyrrell, T., Achterberg, E.P., 2014. Controls on the seasonal variability of calcium carbonate saturation states in the Atlantic gateway to the Arctic Ocean. Mar. Chem. 158, 1–9. https://doi.org/10.1016/j.marchem.2013.10.010.
Urbini, L., Ingrosso, G., Djakovac, T., Piacentino, S., Giani, M., 2020. Temporal and spatial variability of the CO_2 system in a riverine influenced area of the Mediterranean Sea, the Northern Adriatic. Front. Mar. Sci. 7, 679. https://doi.org/10.3389/fmars.2020.00679.
van Geen, A., Boyle, E.A., Moore, W.S., 1991. Trace metal enrichments in waters of the Gulf of Cadiz, Spain. Geochim. Cosmochim. Acta 55, 2173–2191. https://doi.org/10.1016/0016-7037(91)90095-M.
Vargas-Yáñez, M., Viola, T.S., Jorge, F.P., Rubín, J.P., García, M.C., 2002. The influence of tide-topography interaction on low-frequency heat and nutrient fluxes, application to Cape Trafalgar. Cont. Shelf Res. 22, 115–139. https://doi.org/10.1016/S0278-4343(01)00063-2.
Waldbusser, G.G., Hales, B., Langdon, C.J., Haley, B.A., Schrader, P., Brunner, E.L., Gray, M.W., Miller, C.A., Gimenez, I., 2015. Saturation-state sensitivity of marine bivalve larvae to ocean acidification. Nat. Clim. Chang. 5, 273–280. https://doi.org/10.1038/nclimate2479.
Wallace, R.B., Baumann, H., Grear, J.S., Aller, R.C., Gobler, C.J., 2014. Coastal ocean acidification: the other eutrophication problem. Estuar. Coast. Shelf Sci. 148, 1–13. https://doi.org/10.1016/j.ecss.2014.05.027.
Wanninkhof, R., Barbero, L., Byrne, R., Cai, W.J., Huang, W.J., Zhang, J.Z., Baringer, M., Langdon, C., 2015. Ocean acidification along the Gulf Coast and East Coast of the USA. Cont. Shelf Res. 98, 54–71. https://doi.org/10.1016/j.csr.2015.02.008.
Wootton, J.T., Pfister, C.A., Forester, J.D., 2008. Dynamic patterns and ecological impacts of declining ocean pH in a high-resolution multi-year dataset. Proc. Natl. Acad. Sci. U. S. A. 105, 18848–18853. https://doi.org/10.1073/pnas.0810079105.
Xue, L., Cai, W.J., Hu, X., Sabine, C., Jones, S., Sutton, A.J., Jiang, L.Q., Reimer, J.J., 2016. Sea surface carbon dioxide at the Georgia time series site (2006–2007): air-sea flux and controlling processes. Prog. Oceanogr. 140, 14–26. https://doi.org/10.1016/j.pocean.2015.09.008.
Xue, L., Cai, W.J., Sutton, A.J., Sabine, C., 2017. Sea surface aragonite saturation state variations and control mechanisms at the Gray's Reef time-series site off Georgia, USA (2006–2007). Mar. Chem. 195, 27–40. https://doi.org/10.1016/j.marchem.2017.05.009.
Zeebe, R.E., Wolf-Gladrow, D.A., 2001. CO_2 in seawater: equilibrium, kinetics, isotopes. Elsevier Oceanography Series, Amsterdam (347 pp.).
Zhai, W.D., Zheng, N., Huo, C., Xu, Y., Zhao, H.D., Li, Y.W., Zang, K.P., Wang, J.Y., Xu, X.M., 2014. Subsurface pH and carbonate saturation state of aragonite on the Chinese side of the North Yellow Sea: seasonal variations and controls. Biogeosciences 11, 1103–1123. https://doi.org/10.5194/bg-11-1103-2014.
Zhai, W.D., Zheng, L.W., Li, C.L., Xiong, T.Q., Wang, S.Y., 2020. Changing nutrients, dissolved oxygen and carbonate system in the Bohai and Yellow Seas, China. In: Chen, C.T.A., Guo, X. (Eds.), Changing Asia-Pacific Marginal Seas. Atmosphere, Earth, Ocean and Space. Springer, Singapore, pp. 121–137 https://doi.org/10.1007/978-981-15-4886-4_8.